ELSEVIER

Journal of Structural Geology 28 (2006) 1496–1519

JOURNAL OF STRUCTURAL GEOLOGY

www.elsevier.com/locate/jsg

Transpression and strain partitioning in the Caribbean Island-arc: Fabric development, kinematics and Ar–Ar ages of syntectonic emplacement of the Loma de Cabrera batholith, Dominican Republic

J. Escuder Viruete [a,*], F. Contreras [b], G. Stein [c], P. Urien [c], M. Joubert [c], T. Ullrich [d], J. Mortensen [d], A. Pérez-Estaún [e]

[a] *Instituto Geológico y Minero de España, Ríos Rosas 23, 28003 Madrid, Spain*
[b] *INYPSA, C. Velásquez - 69, 28001 Madrid, Spain*
[c] *BRGM, Av. C. Guillemin, 45060 Orléans, France*
[d] *Pacific Centre for Isotopic and Geochemical Research, University of British Columbia, 6339 Stores Road, Vancouver, BC V6T 1Z4, Canada*
[e] *I.C.T. Jaume Almera-CSIC, Lluís Solé i Sabarís s/n, 08028 Barcelona, Spain*

Received 28 June 2005; received in revised form 17 April 2006; accepted 19 April 2006
Available online 12 July 2006

Abstract

An integrative structural and geochronologic study of the Loma de Cabrera batholith (LCB, Cordillera Central, Dominican Republic) and its country rocks reveals the interplay of deformation, metamorphism and plutonism produced in the Caribbean island-arc during Late Cretaceous oblique convergence. The results emphasize the interference between three contemporaneous strain fields: (1) a northern and southern domains produced by (<95 Ma) arc-perpendicular NE- and SW-vergent folding and thrusting, respectively; (2) arc-parallel sinistral strike-slip shearing along the La Meseta shear zone (LMSZ), active during the 88–74 Ma interval; and (3) the adjacent syn-kinematic emplacement of the LCB (90–74 Ma; $^{40}Ar/^{39}Ar$ in hornblende) during sinistral transpressional shearing. Comparison of the structural data with strain models of oblique plate convergence suggest that the LMSZ is a preserved ductile signature of strike-slip partitioning within a sinistral transpressional intra-oceanic subduction zone. In the LCB, microstructural data indicate that the magmatic to high-temperature solid-state deformation initially occurred over a wider band of heterogeneously distributed shear deformation, and was partitioned in narrow bands of mid- to low-temperature deformation connected with the LMSZ during the cooling of the batholith. Field and geochronologic studies also suggest that shortening across the southern domain took place concurrently with sinistral strike-slip movement along the crustal-scale La Guácara and Macutico fault zones, also consistent with a transpressional setting for the Late Cretaceous Caribbean magmatic arc. Shear and fault zones were variably reactivated during Upper Eocene-Oligocene thrusting and Miocene to Recent uplift of the Cordillera Central.

Keywords: Transpression; Strain partitioning; Batholith emplacement; Oblique plate convergence; Caribbean magmatic arc

1. Introduction

The 3-D structure of an island-arc above an obliquely subducting oceanic plate is generally characterized by a forearc region dominated by normal shortening deformation and a strike-slip fault system in/or adjacent to the volcanic axis (Fitch, 1972; Dickinson and Seely, 1979; Jarrard, 1986). As a consequence, the resulting structural pattern is driven by transpression: the arc-perpendicular component of transpression being recorded by folds and thrusts located in the forearc and backarc domains, whilst the arc-parallel slip component of transpression is recorded in steeply dipping or subvertical crustal scale shear zones through the entire arc (Megard, 1987; MacCaffrey, 1991; Teyssier et al., 1995; Tikoff and

* Corresponding author. Instituto Geologico Minero España, Area Geología y Geofísica, C. La Calera 1, 28760 Tres Cantos, Madrid, Spain. Tel.: +34 9172 87242.
E-mail address: j.escuder@igme.es (J. Escuder Viruete).

0191-8141/$ - see front matter © 2006 Elsevier Ltd. All rights reserved.
doi:10.1016/j.jsg.2006.04.003

De Saint Blanquat, 1997; Lallemand et al., 1999; Chemenda et al., 2000; Chardon, 2003).

In oblique subduction zones, magmatic arcs are continuous zones of high heat flow into which melts (or fluids) are continually injected, resulting in a thermally activated zone of lithospheric weakness (Jarrard, 1986; Brown and D'Lemos, 1991; Hutton and Reavy, 1992; McCaffrey, 1992). Therefore, the locus of active magmatism should accommodate the strike-slip component of oblique convergence by developing subvertical shear zones (Petford and Atherton, 1992; Bellier and Sebrier, 1994; De Saint Blanquat et al., 1998). As described by many authors, the simultaneous combination of normal shortening deformation within the arc, which produces fold and thrust structures, and plutons emplaced along subparallel strike-slip shear zones, suggests an overall transpressional setting for arc magmatism (Crawford and Crawford, 1991; Hutton and Reavy, 1992; Ingram and Hutton, 1994; Tikoff and De Saint Blanquat, 1997).

In this paper, the interplay of transpression and plutonism at mid-crustal levels of an intra-oceanic arc is examined by studying the structural relations between the Loma de Cabrera batholith (LCB) and its country rocks in the NW Cordillera Central, Dominican Republic. This is one of the largest plutonic complexes of the arc formed by oblique subduction along the northern edge of the Caribbean plate during the Late Cretaceous (Lewis, 1982; Feigenson, 1978; Cribb, 1986; Draper and Lewis, 1991; Kesler et al., 1991; Donnelly et al., 1994). The recent detailed structural and petrological mapping of the LCB in the context of a regional cartographic project funded by the European Union (SYSMIN project; Contreras et al., 2004; Escuder Viruete et al., 2004; Joubert et al., 2004; Urien et al., 2004), combined with microstructural studies and Ar–Ar geochronology, have shown a geometric, kinematic and temporal continuity between the magmatic intrusion, solid-state deformation of the batholith and the development of the >85 km long La Meseta shear zone (LMSZ). Distribution of structures and kinematics support a model of transpression and strain partitioning during the emplacement of the LCB in the Late Cretaceous (88–74 Ma).

2. Geodynamic setting

2.1. The Caribbean island-arc in Hispaniola

Located in the northern margin of the Caribbean plate (Fig. 1), the tectonic collage of Hispaniola results from the WSW to SW-directed oblique-convergence of the continental margin of the North American plate with the Cretaceous Caribbean island-arc system, which began in Eocene to Early Miocene times and continues today (Donnelly et al., 1990; Lewis and Draper, 1990; Draper et al., 1994; Mann, 1999). Hispaniola has been divided into tectonostratigraphic terranes based on their different geological history (Mann et al., 1991), tectonically placed together by post-Eocene/Oligocene strike-slip, WNW–ESE fault zones. These are the Septentrional (SFZ), Hispaniola (HFZ), Bonao-La Guácara (LGFZ), San Juan-Restauración (SJRFZ) and Enriquillo-Plantain Garden (EPGFZ) fault zones (Fig. 1). The arc-related rocks are regionally overlain by Upper Eocene to Holocene siliciclastic and carbonate sedimentary rocks that post-date island-arc

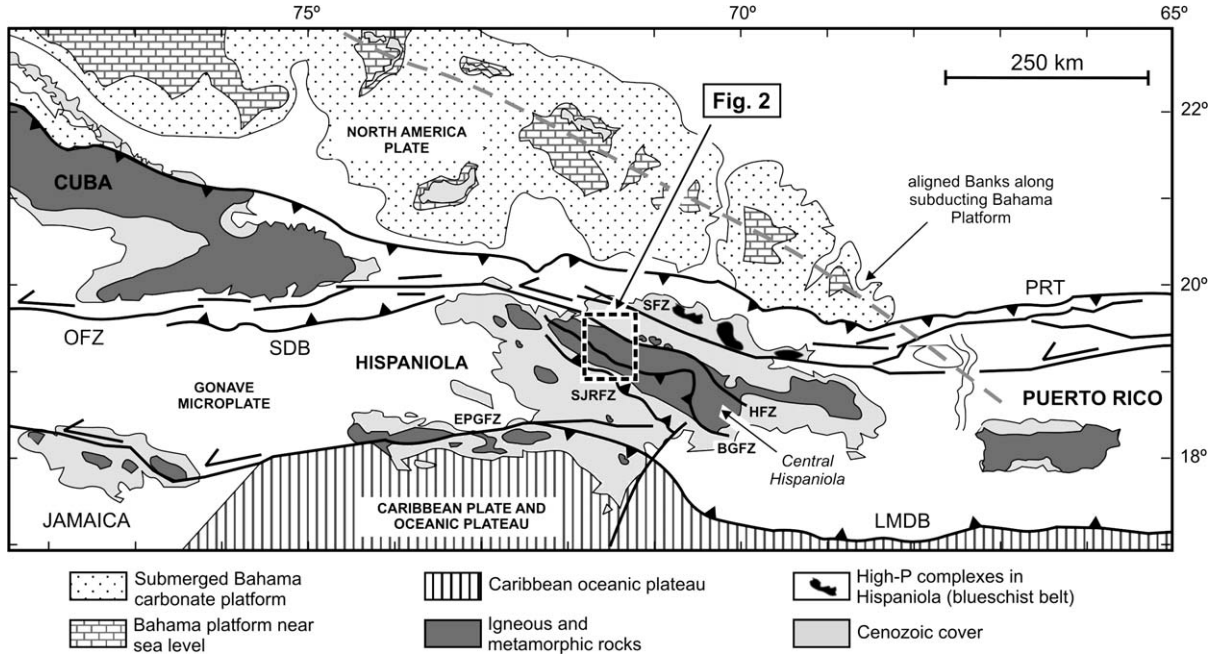

Fig. 1. Map of the northeastern Caribbean plate margin modified from Dolan et al. (1998). OFZ, Oriente Fault Zone; SDB, Santiago deformed belt; EPGFZ, Enriquillo-Plantain Garden fault zone; SFZ, Septentrional fault zone; HFZ, Hispaniola fault zone; BGFZ, Bonao-La Guácara fault zone; SJRF, San Juan-Restauración fault zone; PRT, Puerto Rico trench; LMDB, Los Muertos deformed belt. Central Hispaniola is bound by HFZ and BGFZ. Box shows map of the northwestern Cordillera Central, Dominican Republic, in Fig. 2.

magmatic activity and record the oblique arc-continent collision in the north, as well as the active subduction in the southern Hispaniola margin (Dolan et al., 1998; Mann, 1999).

Central Hispaniola (Fig. 1) is a composite of oceanic derived units bound by the left-lateral strike-slip Hispaniola and Bonao-La Guácara fault zones (Fig. 1). South of the HFZ, in the Cordillera Central, accreted units mainly include the Late Jurassic Jarabacoa-La Vega unit, with the Loma Caribe serpentinized peridotite, N-MORB gabbros and basalts, and pelagic sediments; the Lower Cretaceous oceanic plateau represented by the Duarte Complex; and the Upper Cretaceous arc-related igneous and metamorphic rocks of the Tireo Formation (Bowin, 1975; Mann et al., 1991; Draper and Lewis, 1991; Draper et al., 1994; Lapierre et al., 1999; Lewis et al., 2002; Escuder Viruete et al., 2004). The structure of Central Hispaniola is characterized by the presence of folds, thrust, and left-lateral subvertical faults and shear zones. This deformation is coeval with intrusion of syn- to late-kinematic gabbro-tonalitic batholiths in the Upper Cretaceous. Sedimentary basins filled with the Magua-Tavera Formation (Contreras et al., 2004) and unconformably deposited over these structures, particularly the Hispaniola fault zone, and the intrusion of plutonic units, indicate that the main structure of Central Hispaniola was pre-Eocene/Oligocene.

Cenozoic eastward movement of the Caribbean plate relative to the southern part of the Bahamas Platform has led to collision and deformation in the forearc, intra-arc and backarc volcano-sedimentary basins, and Upper Miocene-Recent topographic uplift in Hispaniola (Dolan et al., 1991, 1998; Mann et al., 1995). In south Central Hispaniola, convergence reactivated Upper Cretaceous structures and lead to the formation of the Upper Eocene-Oligocene SW-vergent Peralta fold-and-thrust belt, the associated San Juan foreland basin and the Neogene thrust bound ramp or push-down Azua basin (Hernaiz Huerta and Pérez-Estaún, 2002; Díaz de Neira and Solé Pont, 2002).

2.2. Structural domains in the Cordillera Central

The structure of the NW area of the Cordillera Central is characterized by several subvertical fault zones that trend WNW–ESE and have a sinistral strike-slip sense of movement, and bound three structural domains (Figs. 2 and 3; Contreras et al., 2004; Stein et al., 2004; Urien et al., 2004). These structures are the Hispaniola, La Meseta (LMSZ), La Guácara (LGFZ), Macutico (MFZ) and San José-Restauración (SJRFZ) fault zones. The HFZ is the longest tectonic feature affecting whole Hispaniola and place together the Amina-Maimón schist belt against the units of the Cordillera Central (Draper and Lewis, 1991). In the area studied, serpentinite lenses equivalent to Loma Caribe serpentinized peridotite occur in the northern boundary of the HFZ, which were tectonically interleaved with Cordillera Central rocks during at least Late-Eocene to Present deformation. Sinistral strike-slip motion took place in the HFZ across a 1–3 km wide mylonitic deformation zone produced by ductile to ductile-brittle shearing (Draper and Lewis, 1991; Contreras et al., 2004). In map view, this mylonite zone cut at low-angle the traces of the Upper Cretaceous structures developed in the Cordillera Central (see below) and deformed the volcanic and sedimentary rocks of the Paleocene-Oligocene Magua-Tavera Formation.

The area studied comprises a thick sequence of plutonic, volcanic and sedimentary rocks. The rocks were very heterogeneously deformed and metamorphosed to prenhite-pumpellyte, greenschist and amphibolite facies conditions, but the textures of the protoliths are often preserved. From bottom to top, three units have been mapped: (1) a Lower Cretaceous mafic Duarte Complex; (2) the Upper Cretaceous intermediate to silicic extrusive rocks of the Tireo Formation, related with tholeiitic to calc-alkaline arc magmatism and intruded by the gabbro to tonalite batholiths of Loma de Cabrera, Loma del Tambor and Macutico; and (3) the basalts of Pelona-Pico Duarte Formation. This magmatic sequence is interpreted to constitute the crustal section of an oceanic island-arc that was built on the proto-Caribbean oceanic crust represented by the Jarabacoa-La Vega unit and the overlying Duarte Complex (Escuder Viruete et al., 2004). The end of arc magmatism is recorded by the deposition of the shallow-water limestone of the Nalga de Maco Formation during Middle to Late Eocene time (Contreras et al., 2004).

2.3. Geology of the Loma de Cabrera batholith and its country rocks

The Loma de Cabrera batholith has a WNW–ESE asymmetric elongate outcrop, measuring 80 km in length by 30 km in width. It is subparallel to the regional structure of the Cordillera Central. In the Dajabón area and in Haiti, the LCB is partially covered by recent sediments. Compositionally, the LCB is multiphase, composed of a heterogeneous suite of plutonic rocks that can be grouped into four mappable units (Fig. 2; Lewis, 1982; Feigenson, 1978; Cribb, 1986; Contreras et al., 2004; Escuder Viruete, 2004; Urien et al., 2004): (1) ultramafic rocks; (2) gabbro-diorite; (3) hornblende ± biotite-bearing tonalite; and (4) a mafic dike swarm. Locally, units (1) and (2) were mapped in a gabbro-ultramafic complex. Surface exposures of ultramafic rocks vary in extent from 0.1 to 10 km^2. They form lenticular massifs and scattered small bodies enclosed in the gabbro-diorite unit, as Loma Chacuey, Loma los Mameyes, Cerro del Pescado, Lomas Altas and Loma Guazumito-Los Charamicos (Fig. 2). The ultramafic rocks have a broad compositional range, including websterite, wehrlite, olivine clinopyroxenite, lherzolite, hornblende-olivine clinopyroxenite, plagioclase-bearing hornblende-clinopyroxenite and hornblendite. In general, these ultramafic rocks are massive and unfoliated. However, modal compositional variations of olivine, clinopyroxene, plagioclase and orthopyroxene define subtle to conspicuous layering of cumulate origin, which ranges in scale from centimeters to meters. The common late magmatic replacement of clinopyroxene by brown hornblende indicates a late-stage enrichment of H_2O in the intercumulus liquid.

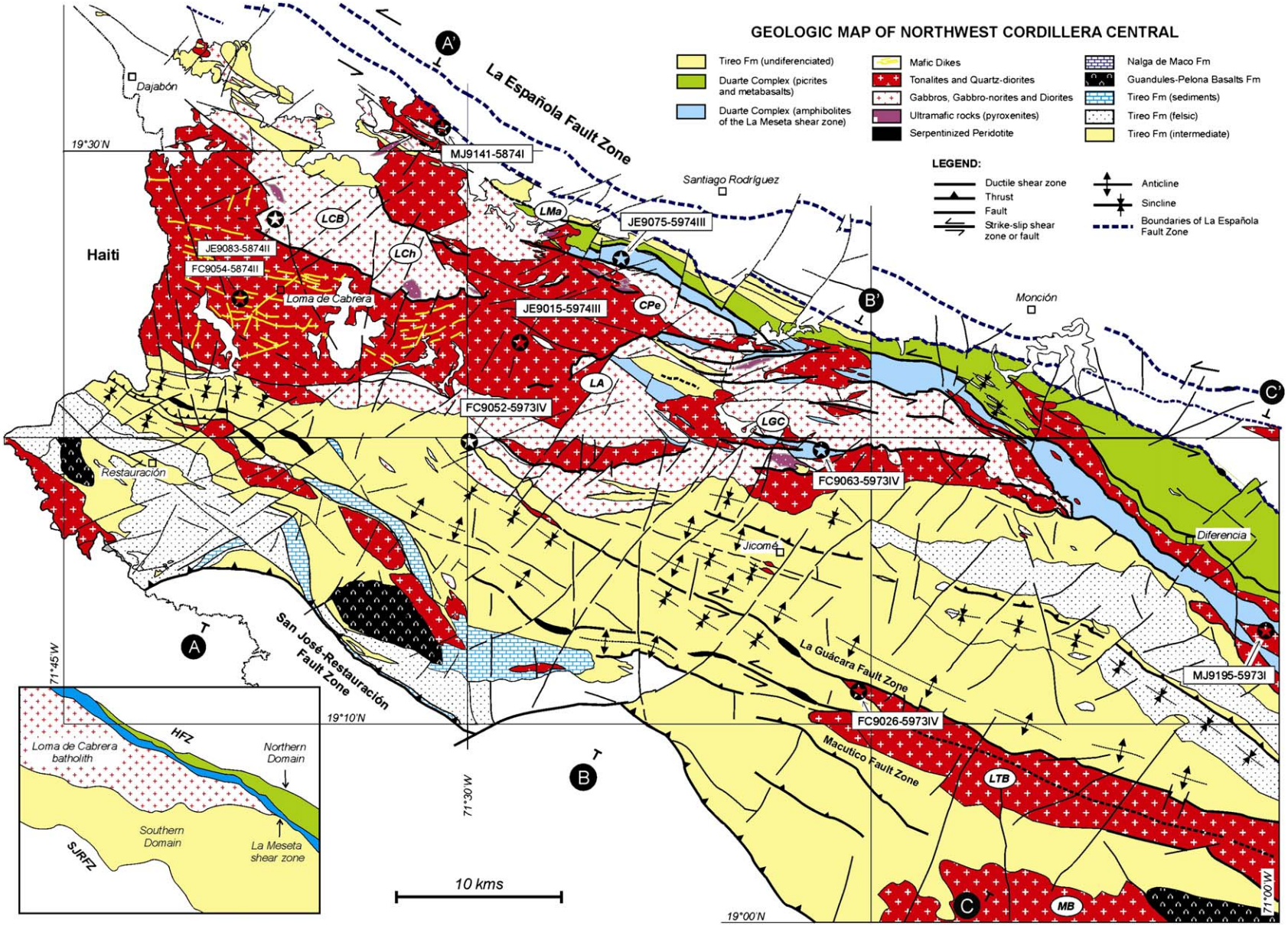

Fig. 2. Geological map of the NW Cordillera Central, Dominican Republic (Contreras et al., 2004; Joubert et al., 2004; Stein et al., 2004; Urien et al., 2004). LCB, Loma de Cabrera batholith; LTB, Loma del Tambor batholith; MB, Macutico batholith. Ultramafic-gabbroic massifs: Loma Chacuey (LCh), Loma los Mameyes (LMa), Cerro del Pescado (CPe), (SYSMIN Project). Lomas Altas (LA) and Loma Guazumito-Los Charamicos (LGC). In the figure, A−A′, B−B′ and C−C′ are the geological cross-sections of the Fig. 3. Text labels in boxes show location of samples selected for $^{40}Ar/^{39}Ar$ geochronology.

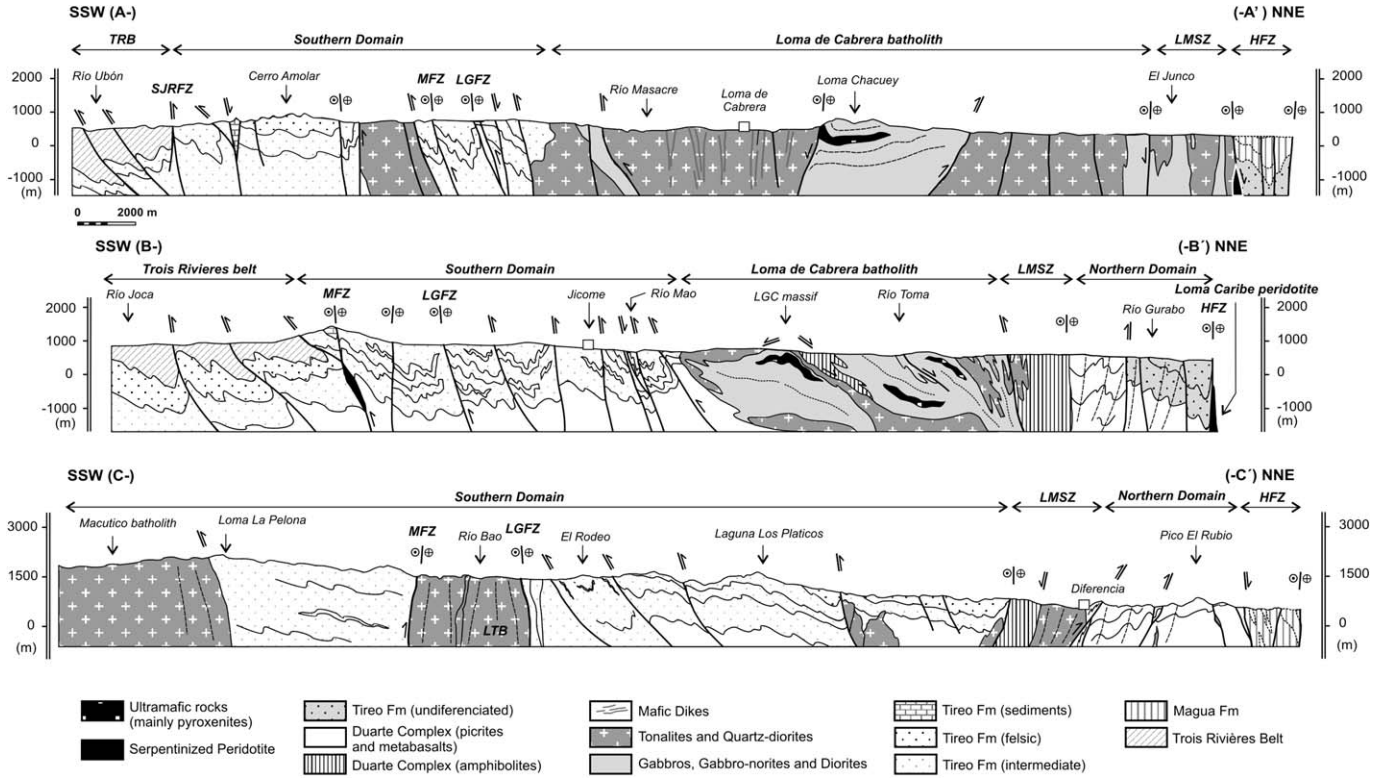

Fig. 3. Geologic cross-sections through the NW Cordillera Central showing the structural relations between the northern domain, La Meseta shear zone, the Loma de Cabrera batholith and the southern domain.

The gabbro-diorite unit is composed of several elongate plutons separated by outcrops of hornblende tonalite. A heterogeneous texture and composition characterize the gabbro-diorite unit. This heterogeneity, plus local intrapluton intrusive relationships, suggests that the gabbro-diorite unit evolved during a piecemeal intrusive history. Individual gabbroic bodies may be within the large, undivided gabbro-diorite; however, rock weathering and vegetation cover make their delineation very difficult. The gabbro-diorite unit varies from hornblende-augite gabbro to hornblende diorite. Some parts of the unit are hornblende rich, characterized by local variations in modal composition as well as textures ranging from medium-grained hornblende diorite-gabbro to pegmatitic types and isolated patches of hornblendite (produced by H_2O-rich fluids). Other gabbroic types occur as non-equigranular gabbronorite and melanogabbro. Igneous layering occurs in the gabbroic rocks, which is defined by alternating bands of mafic minerals (augite and hornblende) and calcic plagioclase. In some dioritic rocks, hornblende and biotite define a magmatic foliation ± lineation.

The hornblende ± biotite-bearing tonalite forms a complex, WNW–ESE to W–E-elongated body, with minor aligned plutons that intruded the gabbro-diorite unit. In detail, it is texturally very heterogeneous (Feigenson, 1978; Cribb, 1986). The tonalite unit is traceable at the surface from NW Diferencia westward to Dajabón, and continues into Haiti. Typically, the contact between the younger tonalite and the enclosed gabbro-diorite unit is a ductile deformation zone, characterized by magmatic to solid-state textures in the tonalite and solid-state textures in the gabbro and diorite (Fig. 4a,h; see below). However, gabbroic and dioritic xenoliths occur in the tonalites, and tonalitic dikes intrude into the adjacent gabbro-diorite unit, clearly indicating a younger age for the tonalite suite (Fig. 4a,c). Texturally, the tonalitic rocks are mainly medium- to coarse-grained (1–5 mm), hypidiomorphic granular and are non-foliated to strongly foliated (Fig. 4b,d). A typical hornblende tonalite consists of subhedral oscillatory-zoned plagioclase, anhedral quartz and acicular to prismatic, olive-green hornblende with accessory apatite, Fe–Ti oxides, titanite and zircon. Some facies also contain subhedral biotite and rare K-feldspar. The tonalitic rocks grade in sectors into quartz-bearing hornblende diorite. White-weathering plagioclase-phyric biotite tonalite, leucogranite microporphyry and aplite occurs as late dikes in the mainly tonalitic intrusion.

A late stage mafic dike swarm is intruded into the LCB and its country rocks. The mafic dikes have a general high-angle of dip (>60°; Fig. 4a), but vary in strike. Two main sets are recognized: WNW–ESE to W–E, subparallel to the elongation of the tonalite unit; and NE–SW to ENE–WSW (see below). At outcrop scale, many mafic dikes appear to be planar and have chilled margins. Some are intruded subparallel to the magmatic foliation in the tonalites. Petrographically, the most common dike lithotype is aphyric hornblende microdiorite. Other types include clinopyroxene + hornblende-phyric gabbro, clinopyroxene-phyric diabase, hornblende microdiorite

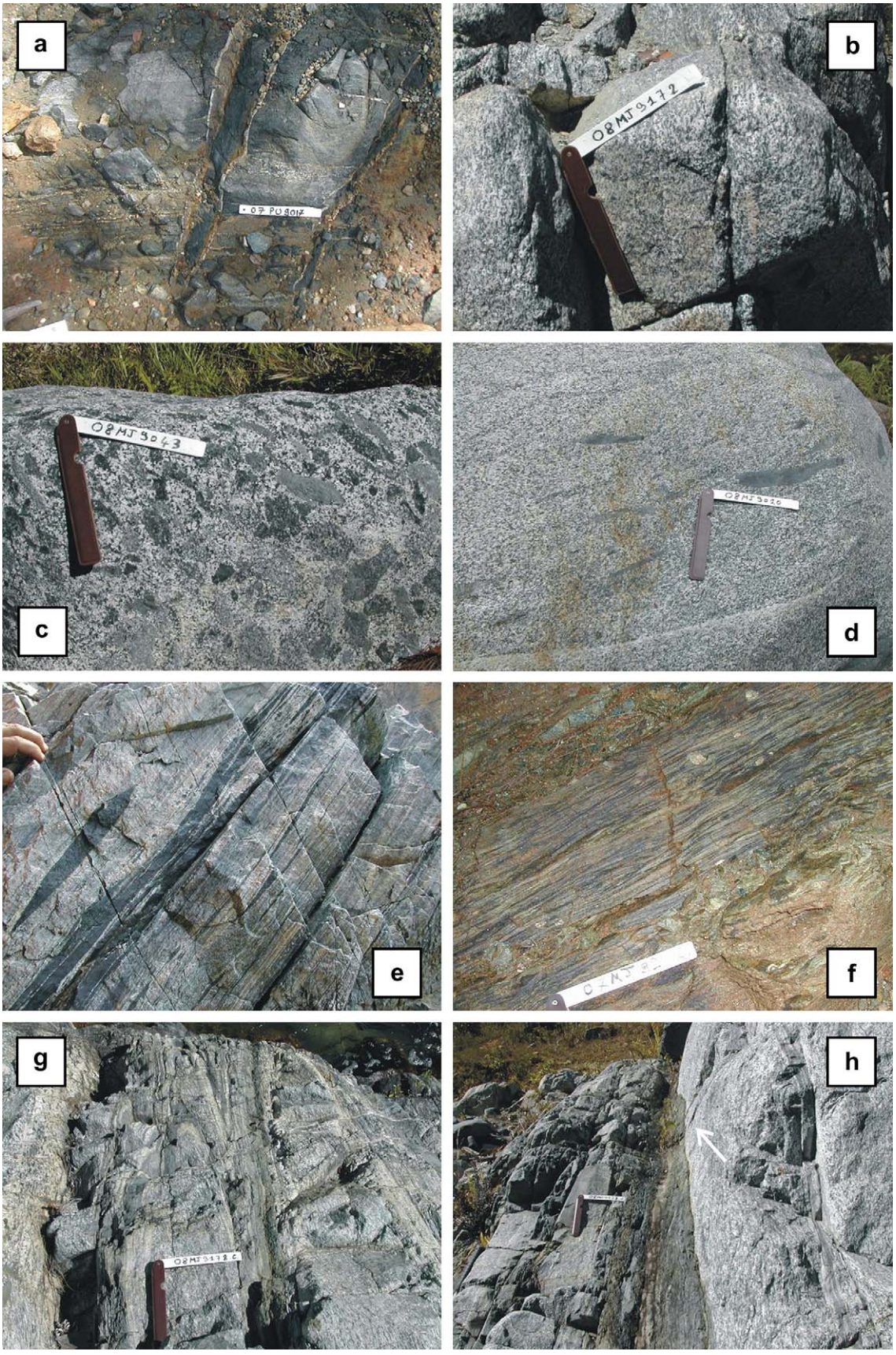

Fig. 4. Field aspect of magmatic and solid-state structures in the Loma de Cabrera batholith and its country rocks: (a) Subvertical shearing and boudinage of syn-kinematic hornblende-bearing tonalite dikes within fine-grained foliated gabbro. Loma Guazumito-Los Charamicos massif. High-T subvertical foliation in gabbro has a WNW-trend and is cut by NE-trending subvertical late mafic dikes; (b) Subvertical magmatic foliation (N120°E−80°SW) in coarse-grained, hornblende-tonalite. Río Baito; (c) Subparallel elongated enclaves of hornblendite and gabbro/diorite defines the magmatic foliation in coarse-grained, hornblende tonalite; (d) Magmatic to local high-T solid-state foliation developed in hornblende-tonalite. Note the hornblende grain-shape fabric and the foliation defined by elongated

and plagioclase + hornblende-phyric diorite porphyry. The late mafic dikes have a subduction-related signature (Escuder Viruete, 2004) and are locally intermingled with the hornblende tonalite. Irregular deformed pods of geochemically similar rock types also occur within the tonalite and are interpreted to represent dismembered dikes or the product of magma mixing.

Several geochronologic techniques have been used previously to date the plutonic units of the LCB. Rb–Sr dating of the tonalite unit in the central-western area gives a whole rock crystallization age of 90 Ma (Feigenson, 1978). Hornblende K–Ar ages of 127 Ma for the El Pino diorite and 67 ± 9 and 48.2 ± 6 Ma for two tonalite samples were obtained by Kesler et al. (1991). In tonalites of the central-eastern area of the LCB, $^{40}Ar-^{39}Ar$ analysis on hornblende included in Cribb et al. (1989) yielded plateau ages between 86.5 ± 0.6 and 84.5 ± 1.7 Ma, and $^{40}Ar-^{39}Ar$ plateau ages from biotite yielded ages of 75.3 ± 0.4 and 49.2 ± 0.2 Ma. Taken together, these data indicate a possible Late Cretaceous (Turonian to Santonian) age of intrusion for the tonalites. Country rocks surrounding the LCB consist of very heterogeneously deformed and metamorphosed rocks of the Duarte Complex and Tireo Formation, which form the amphibolites of the LMSZ and an N-dipping roof pendant in the central-eastern sector. In the south area of LCB, these rocks are deformed and intruded by the Loma del Tambor (LTB) and Macutico (MB) batholiths (Contreras et al., 2004; Joubert et al., 2004).

3. Regional-scale structural pattern

A foliation trajectories map (flattening plane) of the LCB and surrounding areas in the Cordillera Central is presented in Fig. 5. It includes more than 700 measurements of magmatic and solid-state foliations in the field and reflects the orientation of the strain ellipsoid. Patterns of finite strain trajectories in the LCB emphasize the synchronism between the internal structure of the batholith, the La Meseta shear zone and regional structures. On a large scale, foliation trajectories are characterized by a dominant WNW–ESE trend along the NE contact of the LCB, parallel to the trace of the LMSZ. From Cerro del Pescado toward the Lomas Altas and south Loma Chacuey areas (Fig. 5), foliation trajectories in the tonalite show a sigmoidal pattern that envelops the Loma Chacuey and Lomas Altas gabbro-ultramafic massifs. In the rest of LCB, the dominant foliation trajectories are oriented WNW–ESE, paralleling the external contact of the batholith. Continuity exists between the internal planar fabrics in the batholith, the metamorphic foliation in the amphibolites of the LMSZ and the regional cleavage and mylonitic fabrics in the country rocks (Fig. 5). At the contact, country rock foliation systematically parallels the foliation in the batholith. No obvious cross cutting relations exist between internal foliation trajectories and the compositional variation in the LCB. The foliation in the deformed external sector of the gabbro-ultramafic massifs generally parallels the intrusive contact and the regional foliation of the tonalite. Internal planar fabrics in the LCB generally have a high-angle of dip (>60°), decreasing progressively toward the SE and eventually becoming shallowly dipping in the central top of the intrusion between Lomas Altas and Cerro del Pescado amphibolitic carapace. East of Diferencia, the deformed SE tail of the LCB is cut by the LMSZ and placed under the Tireo Formation. S-L fabrics in the LMSZ have a high to moderate-dip to the SE, beneath and subparallel to the contact with the LCB.

4. Deformation within and around the batholith

Structural maps of magmatic and solid-state foliation obtained from the field work in the NW Cordillera Central are shown in Figs. 5 and 6. Stereonets of magmatic and solid-state deformative foliation (squares) and mineral/stretching lineation (triangles) are shown in Figs. 7 and 8. Four structural domains are defined in the study area: to the north of the LCB an outcrop with folds and thrust, constituted by the Duarte Complex and the overlying Tireo Formation (including the Dajabón Complex of Draper and Lewis, 1991); to the south of LCB, an area with folds, shear zones and thrusts developed in the Tireo Formation; the Loma de Cabrera batholith; and the amphibolites of the La Meseta shear zone.

4.1. Northern domain

The northern domain pinches out westward in map pattern because it is truncated to the north by the Hispaniola fault zone. There is a gradient in the intensity of the deformation that increases from NE to the SW, from almost undeformed metabasalts of the Duarte Complex south of the El Rubio Peak to strongly sheared schists and amphibolites in the Diferencia area (Fig. 6). The macrostructure comprises several asymmetrical D1 anticlines and synclines with WNW–ESE axes and a NE-vergence, which show long normal limbs and short subvertical (or slightly reversed) limbs, separated in occasions by high-angle reverse faults (C–C′ cross-section; Fig. 3). Associated with D1 folds is an S1 axial-plane cleavage, dipping between 45 and 80° generally to the SW, and

microgranular mafic enclaves; (e) Foliated tonalite with sheared enclaves of amphibolite and mafic dikes, which were rotated into subparallelism with the high-T mylonitic foliation. La Meseta shear zone, Diferencia area; (f) Medium-temperature S-C fabric in sheared Duarte Complex metabasalts. Hornblende remains stable in S-surfaces. S-C fabric and porphyroclast tails asymmetry are dextral (i.e. reverse). Road to Manaclá-Diferencia; (g) Sheared and folded hornblende tonalite of the Macutico batholith intruded along La Guácara fault zone. The structures developed are WNW–ESE-trending asymmetric, isoclinal and often rootless similar-style folds. Axial-planar fabrics in folds contain syntectonic amphibolite facies mineral assemblages. Río Bao; (h) Subvertical contact zone between gabbro and tonalite. Note the solid-state strong deformation in the gabbro and the subparallel magmatic foliation in the tonalite. In thin bands, tonalite is also transformed into L-S tectonite. White arrow shows the low-angle plunge of the magmatic to solid-state lineation in the planar fabric. In all photos white bar scale is 16 cm long.

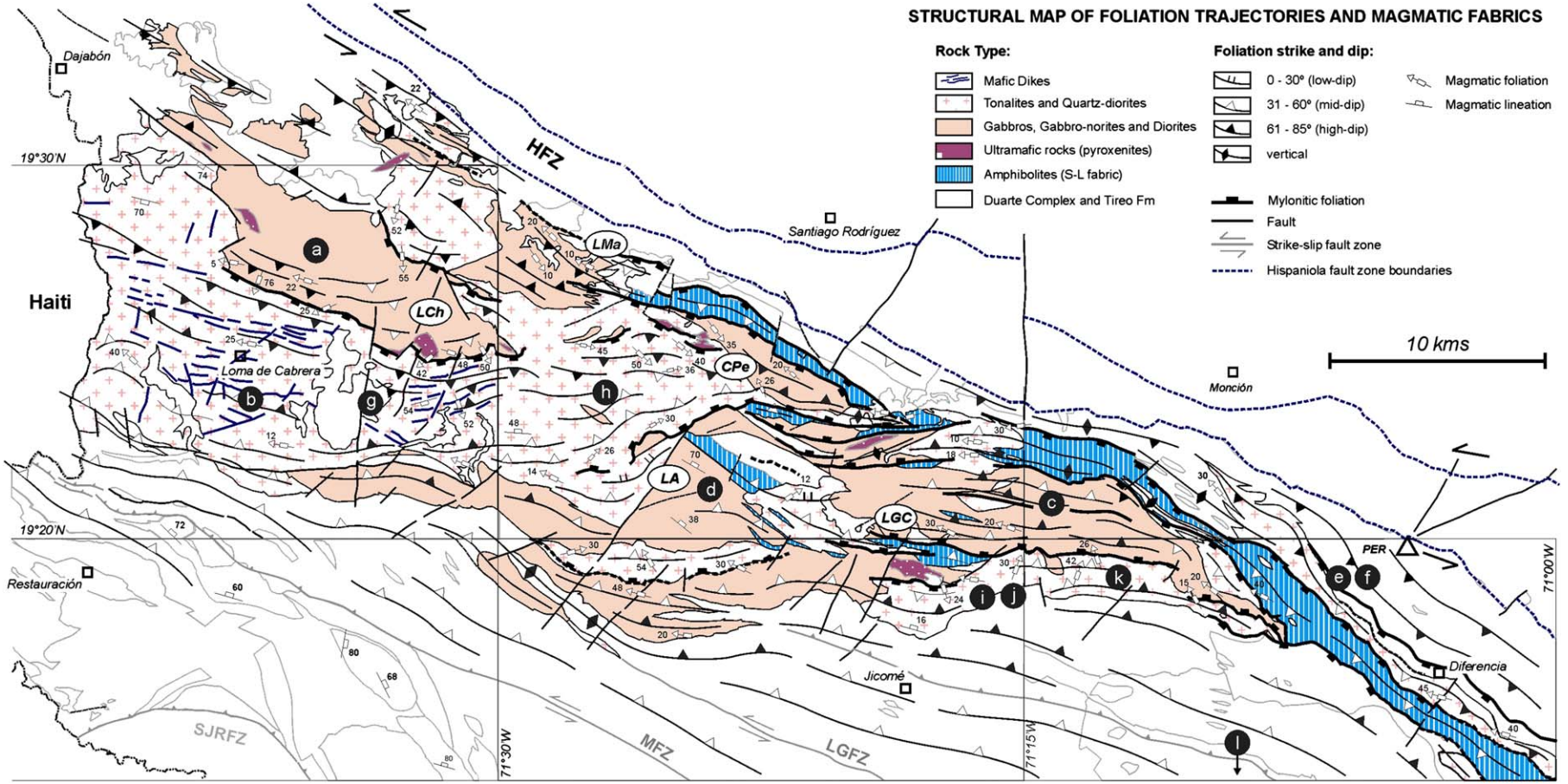

Fig. 5. Structural map of the foliation trajectories and magmatic fabrics in the Loma de Cabrera batholith and surrounding areas based on field studies. Numbered circles refer to specific locations of the stereonets included in Fig. 7 and discussed in the text. PER, El Rubio peak.

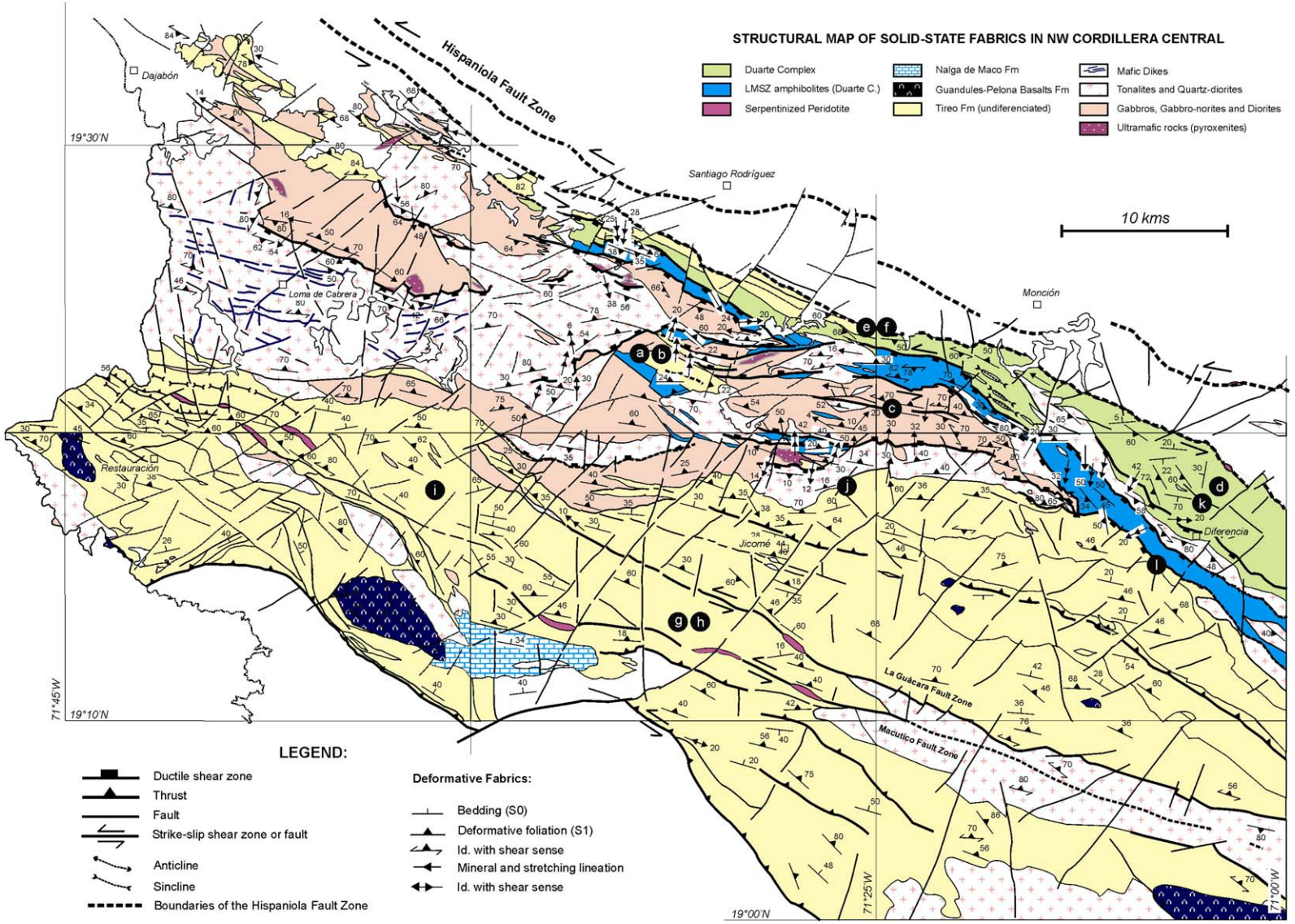

Fig. 6. Structural map of solid-state fabrics in the Loma de Cabrera batholith and surrounding areas based on field studies. Numbered circles refer to specific locations of the stereonets included in Fig. 8 and discussed in the text.

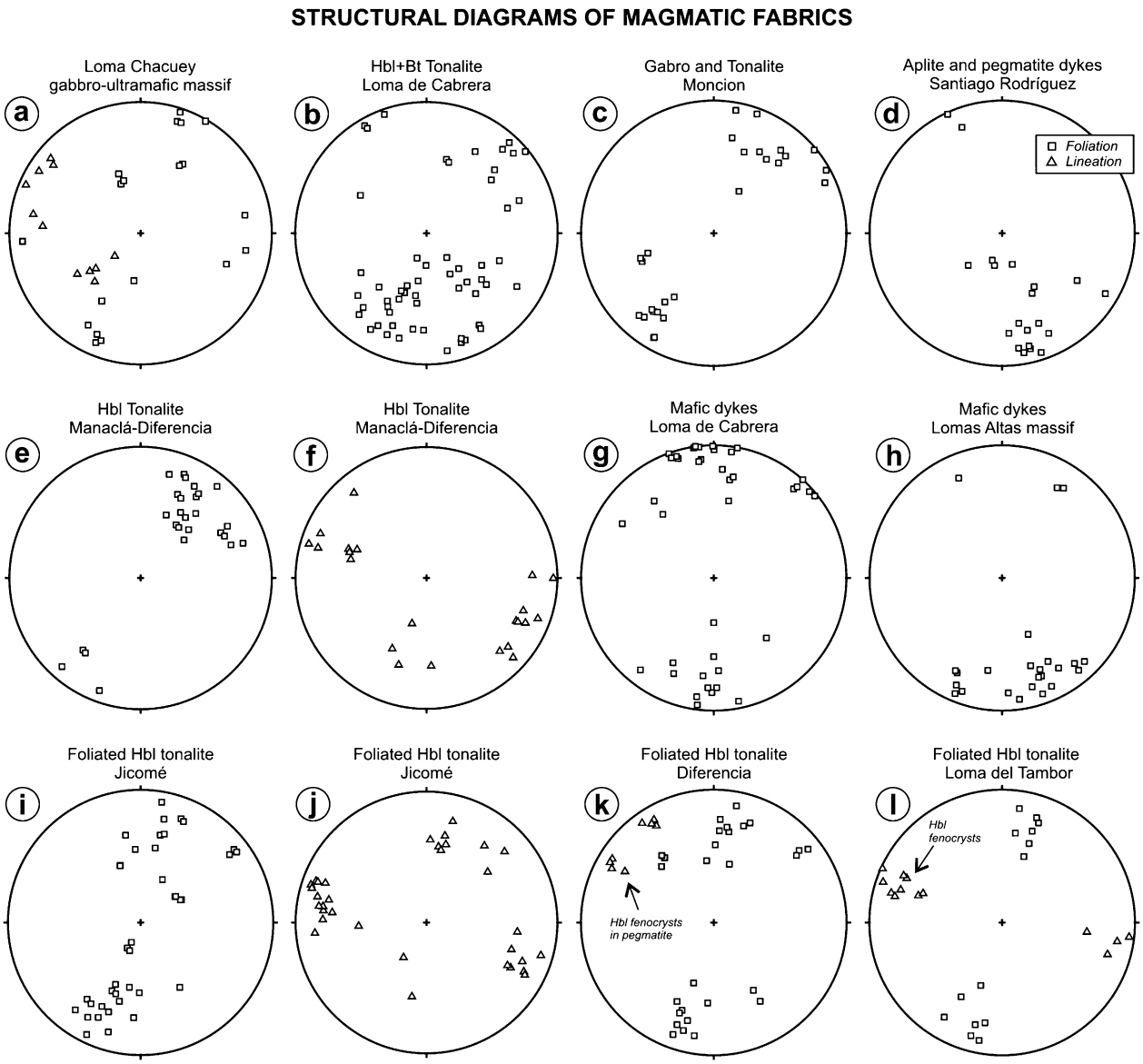

Fig. 7. Stereonets of magmatic foliation (squares) and lineation (triangles) measured in different areas of NW Cordillera Central. Schmidt net, lower hemisphere projection.

a L1 intersection lineation between S1 and the bedding (S0), with a plunge to the NW that is generally less than 20° (Fig. 8d). However, mesoscopic D1 folds are rare because of the poorly defined appearance of bedding in the Duarte Complex metabasalts. S1 cleavage is interpreted as a D1 fabric because in low-strain domains the rocks present undeformed igneous textures. In high-strain areas near the LMSZ, a non-coaxial component of the D1 deformation is expressed locally by shear zones, subparallel to axial-planar foliation of D1 folds. In these shear zones, the protomylonitic to mylonitic foliation is subvertical and contains a WNW–ESE to NW–SE-trending subhorizontal stretching lineation (Fig. 8g,h). The asymmetry of mesoscopic S-C fabrics, boudinage of calcite veins, plagioclase porphyroclasts and mica fish indicates a sinistral subvertical shearing.

4.2. Southern domain

The southern domain is bound by the intrusive contact of the LCB or the La Meseta shear zone to the north and the San José-Restauración fault zone to the south (Fig. 2). The cartographic distribution of the Tireo Formation is defined by an alternation of bands of slightly folded intermediate and felsic metavolcanic rocks with a general dip to the NE, separated by mid- to high-angle thrust faults (Fig. 6; Contreras et al., 2004). The lateral wedging-out of the felsic volcanics and the change of dip in the bedding, suggests the thrust developed footwall synclines and hangingwall anticlines of km-scale cored in the intermediate volcanics. In cross-section B–B′ (Fig. 3), the macrostructure defines a tectonic imbrication of different metavolcanic rocks of the Tireo Formation

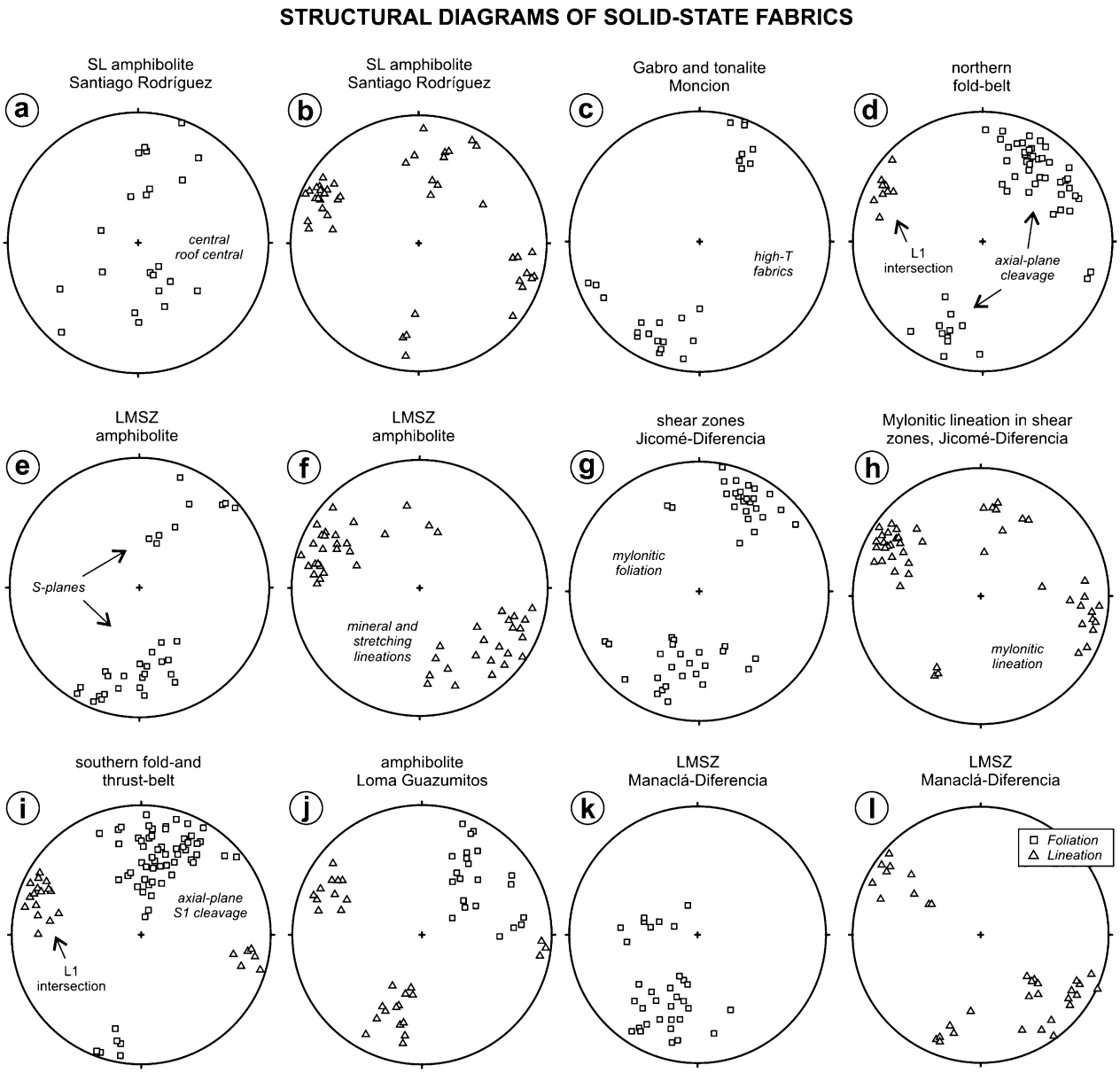

Fig. 8. Stereonets of solid-state foliation (squares) and lineation (triangles) in several localities of the Cordillera Central domain. Orientation of foliation suggests predominantly strike-slip movement within LMSZ. Lineations, defined by stretched minerals in the shear plane, are dominantly subhorizontal throughout shear zone. Schmidt net, lower hemisphere projection.

in a SW-directed fold and thrust belt, with the upper structural levels situated toward the NE. The low-angle pitch of slickensides measured in ductile-brittle to brittle fault surfaces suggests an oblique-sense of movement during thrusting. The southern domain is also affected by the sinistral strike-slip La Guácara and Macutico fault zones. The Loma del Tambor batholith (Fig. 4g) was intruded syn-kinematically along these fault zones, which gave rise its parallel elongate shape and internal subvertical WNW–ESE trending magmatic to solid-state foliation (Fig. 7l,k).

D1 deformation is very heterogeneous in the southern domain. S1 axial-plane fabrics related to the folding (Fig. 8i) are well developed in rocks of the Tireo Formation, where they are phyllites and schists metamorphosed under lower amphibolite to lower greenschist facies conditions. Towards lower structural levels, the D1 deformation is partitioned into thrust and strike-slip subvertical fault surfaces, especially in the La Guácara and Macutico fault zones. Regional syn-kinematic metamorphic conditions are in the prehnite-pumpellyite facies or less. In the Restauración area, the volcanoclastic rocks are generally undeformed (Stein et al., 2004). Consequently, there is a gradient in deformation, which increased from SW to the NE, toward the LCB. Associated with D1 folds there is an L1 intersection lineation between S1 and S0, with a plunge to the NW and SE that is generally less than 20° (Fig. 8i). A non-coaxial component of the D1 deformation is indicated by WNW–ESE to NW–SE-trending subvertical shear zones. In the

Jicomé-Diferencia area, the stereonets of subvertical shear bands and subhorizontal stretching lineation orientations suggest a predominantly strike-slip movement (Fig. 8g,h). The asymmetry of S-C fabrics and tails of plagioclase porphyroclasts in these shear zones, generally indicates a top-to-the NW or WNW shear sense, parallel to the subhorizontal stretching lineation.

4.3. Loma de Cabrera batholith

Within the LCB the foliation and strain is not homogeneously distributed. Weakly foliated tonalites crop out in the core of the batholith, whereas strongly foliated tonalites are located along the northern intrusive contact with the LMSZ amphibolites (Fig. 4e). In order to constrain the timing and conditions of foliation development relative to the tonalitic magma emplacement, a microstructural study was carried out. We have sampled 244 sites covering the LCB as homogeneously as possible. Following Paterson et al. (1989), Tikoff and De Saint Blanquat (1997), and Tikoff et al. (2005), three foliation type zones are recognized on the basis of the field-data (zones 1, 2 and 3 in Fig. 9) and deformation microstructures observed in thin section: magmatic state, high-T solid state, and mid- to low-T solid state ($T < 550$ °C).

Zone 1 refers to slightly deformed igneous rocks with no obvious textural heterogeneities. Gabbro and tonalite are characterized by a preferred orientation of primary igneous minerals formed by magmatic processes that show no evidence of plastic solid-state deformation or recrystallization. In these rocks (Fig. 4b), the magmatic foliation is defined by the preferred planar orientation of euhedral Pl (unbroken; mineral abbreviations are from Kretz, 1983) with aligned twins and oscillatory zoning, that are separated by undeformed large Qtz grains or non-aligned, equant aggregates of Qtz, euhedral Hbl and Pl prisms, and aligned aggregates of fine-grained Hbl and Bt, locally defining a schlieren layering. The magmatic lineation is locally defined by elongation of prismatic Hbl and elipsoidal Qtz and Bt aggregates. The magmatic foliation is also defined in tonalite by the preferred alignment of elongate microgranular mafic enclaves without internal plastic deformation, which we interpreted as incompletely solidified mafic magma globules, and indicates magmatic flow (Fig. 4d). In tonalite, imbrication or tilting of Pl phenocrysts implies non-coaxial magmatic flow involving rotation of crystals in a viscous fluid. In zone 1, the magmatic foliation generally has a WNW–ESE to NW–SE trend and high to moderate dip to the NE and SW (Fig. 7b,i); the plunge of the magmatic mineral lineation is low (Fig. 7a,c). However, foliations with lower dip, where the magmatic lineation have a dip-slip plunge, coexist in sectors of Loma Chacuey, Lomas Altas and Loma Guazumito-Los Charamicos massifs (Figs. 5b and 7a,j).

Zone 2 refers to deformed igneous rocks showing a homogeneous foliation, which bears a weak mineral/stretching lineation. In gabbro and tonalite the foliation is defined by a planar preferred orientation of Pl and Hbl phenocrysts, and is locally accentuated by Bt laminae. The high-T solid-state deformation texture is difficult to differentiate in the field from the magmatic textures, although it involves a slight decrease in the Qtz grain size and a more pronounced shape-preferred orientation of Pl and Hbl. Microstructural changes involve the development of shape-preferred orientations accompanied by a moderate internal deformation of crystals. Qtz grains are slightly elongated, and have lobate shapes, which indicate a high mobility of Qtz grain boundaries and a high-T of solid-state deformation. Likewise, extensive recrystallization of Pl in deformed tonalites implies minimum deformation temperatures >550–600 °C (Passchier and Trouw, 1996). Also, the recovery and recrystallization of Hbl indicates deformation under upper to middle amphibolite facies conditions. High-T solid-state foliation has a general WNW–ESE trend in bands located along the gabbro-tonalite and batholith-country rock intrusive contacts (Figs. 8c and 10a,b). An exception is south of Santiago Rodríguez area (Fig. 8a,b), where bands adopt a different W–E-trend in a shear zone system that connects with the LMSZ. Solid-state stretching lineations are generally shallow plunging in zone 2. However, along strike, the shallow plunge of the lineation is frequently replaced by a down-dip orientation in the foliation plane (Fig. 8j), as in the LMSZ.

Zone 3 refers to a strongly foliated protomylonitic to mylonitic igneous rock, characterized by the association of a relatively homogeneous foliation with small-scale shear bands. At the microscale, the generalization of intracrystalline strain in Qtz and Pl indicate a pervasive solid-state deformation. Although Pl grains are fractured, crystallization of Qtz filling these fractures and matrix quartz grains locally display undulatory extinction. Extensive lobate or mosaic-like patterns of Qtz grains indicate that grain boundary migration and diffusion processes were active. Mylonitic bands with S-C structures developed in tonalite have a gneissic texture that is easily recognizable in the field. These rocks are characterized by a prominent internal deformation, with grain-size reduction along the shear bands, and by development of asymmetric pressure shadows in Pl and Hbl porphyroclasts (Fig. 10c), which typically fracture and undergo boudinage with recrystallized Qtz, Ms, Ab and Chl ± Sph filling the open pull-aparts. In the matrix, mineral grains show evidence of deformation (e.g. undulatory extinction, kinking of Bt), recovery such as subgrain structures in Qtz and recrystallization to finer-grained aggregates. The mylonitic foliation is defined by fine-grained lenticular aggregates of recrystallized Qtz (ribbons), Pl or Bt. This microstructure is broadly indicative of deformation under lower amphibolite to upper greenschist facies conditions (Passchier and Trouw, 1996).

Spatially, zone 3 is located within the zone 2 and near the LMSZ, where deformation is partitioned in mid- to low-T narrow bands (Fig. 9) and the igneous rocks are commonly L or L-S tectonites. High-T solid-state deformation textures occur everywhere in the shear zone system, on both sides of the mylonitic surfaces, often uniformly distributed. The magmatic textures are preserved far from the LMSZ shear zone system. However, rocks in zone 3 characterized by mid- to low-T textures also retain previous high-T and/or magmatic textures. For

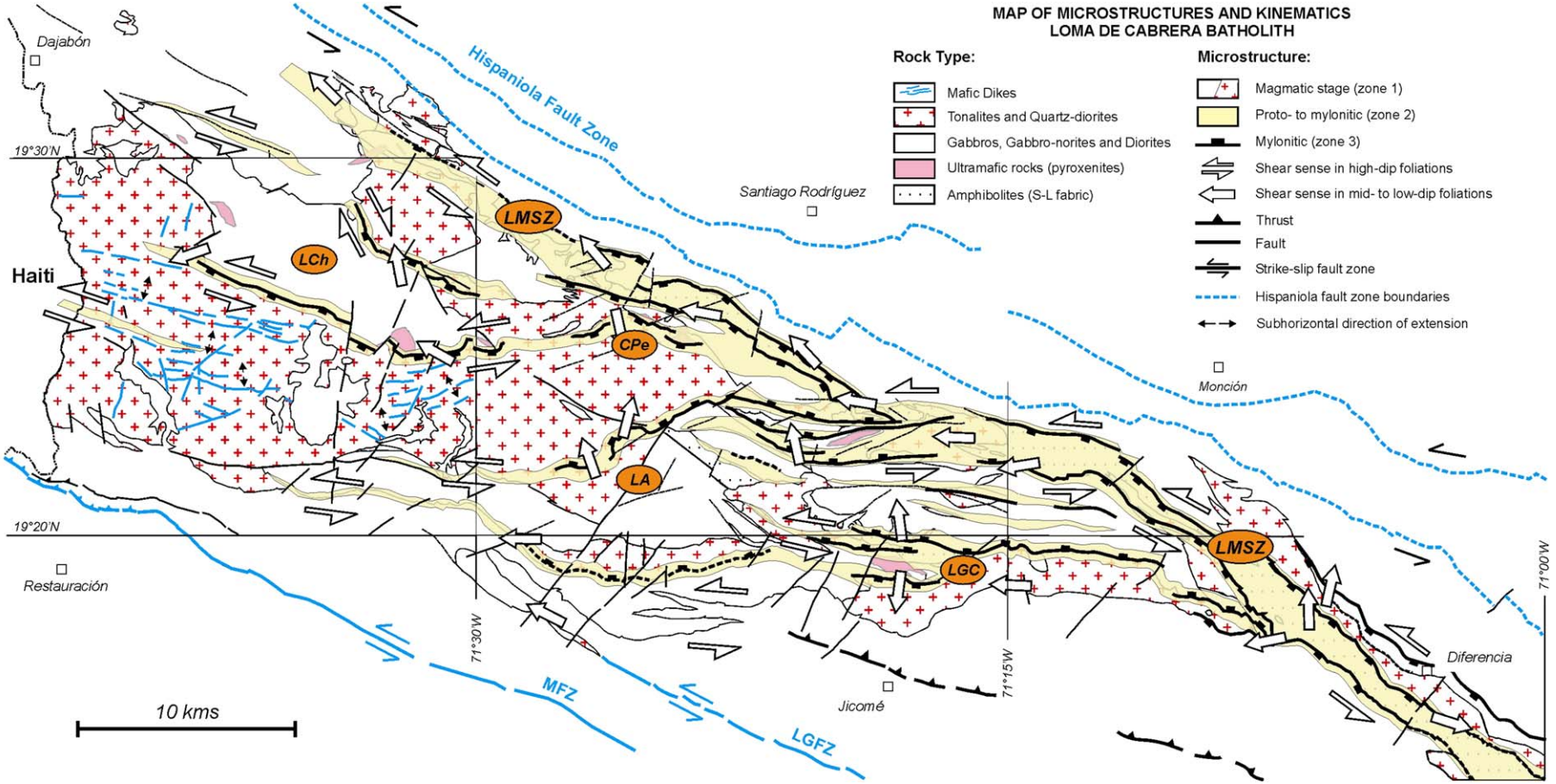

Fig. 9. Structural map of magmatic and solid-state fabrics and kinematics in the Loma de Cabrera batholith and La Meseta shear zone based on field studies. Arrows represent the kinematics of non-coaxial deformation affected the LCB and LMSZ. The geometrical, structural and temporal continuity between the magmatic and solid-state deformations suggest sinistral strike-slip shearing during emplacement of the LCB. Gabro-ultramafic massifs: LCh, Loma Chacuey; LA, Lomas Altas; CPe, Cerro Pescado; LGC, Loma Guazumito-Los Charamicos.

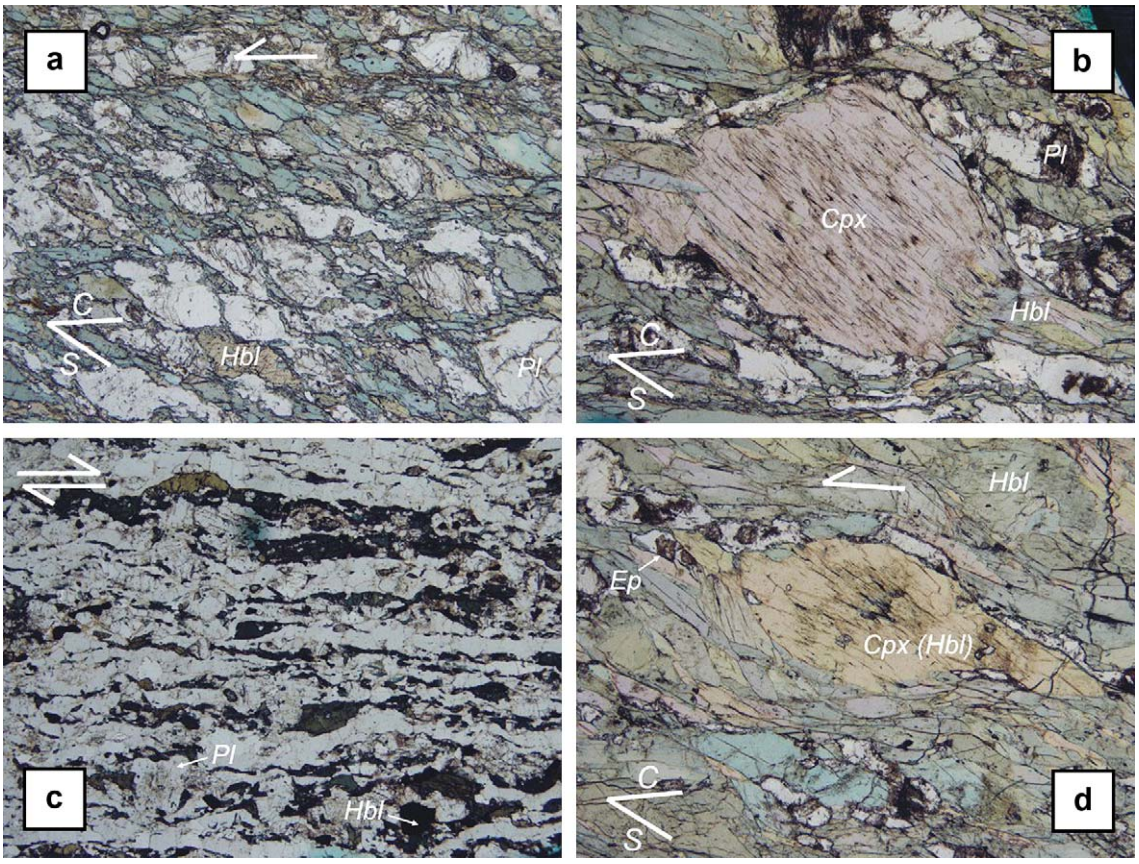

Fig. 10. Loma de Cabrera batholith microstructures (mineral abbreviations from Kretz, 1983). In the microphotographs, the arrows define the shear sense and width of field = 5 mm. (a) Subvertical high-T blastomylonitic fabric in hornblende gabbro of the Loma Chacuey massif. S1 fabric is defined by an alternation of hornblende and plagioclase-rich levels. S-C microstructure and pressure shadows around Pl porphyroclasts defines a sinistral shear sense; (b) Cpx porphyroclasts replaced in rims and pressure shadows by hornblende in gabbroic rocks of the Loma Guazumito-Los Charamicos massif. High-T blastomylonitic fabric is defined by Hbl aligned nematoblasts in S- and C-surfaces; (c) Mid- to low mylonitic fabric in sheared hornblende tonalite, south of Santiago Rodríguez. Elongated Hbl and Pl porphyroclasts are surrounded by a S1-L1 mylonitic fabric defined by aggregates of Pl and Qtz ribbons that show a variable grade of dynamic recrystallization; (d) S1-L1 mylonitic fabric in amphibolites of the La Meseta shear zone developed in epidote-amphibolite metamorphic facies conditions. Note Cpx pseudomorph replaced by Hbl aligned nematoblasts.

example, a preferred alignment of elongate mafic enclaves are preserved in low strain domains surrounded by sheared tonalite with a subparallel S-C structure, or spaced shear bands bound domains on a scale of centimeters with preserved high-T microstructures. The latest deformation took place in low-T, solid-state conditions, as evidenced by the greenschist facies microstructures. These data indicate that the magmatic to high-T solid-state deformation initially occurred over a wider band of heterogeneously distributed shear deformation (Fig. 11). Also, the data suggests a localization of strain with increasing solid-state deformation in the zone 3 narrow bands during a decrease of temperature linked to the cooling history of the LCB. The westward branching of the LMSZ into a system of W–E trending shear zones produces local NNW- and SSE-directed extensional movements at the top of the batholith and around some gabbroic-ultramafic massifs (Fig. 9).

4.4. Amphibolites of the La Meseta shear zone

The LMSZ forms a continuous, 1–3 km thick, southward-dipping belt of amphibolitic rocks that outcrop between Diferencia and Dajabón (Figs. 5, 6). The southern boundary of this WNW–ESE to NW–SE belt of amphibolites is commonly a sharp and strongly deformed contact with the gabbro-diorite unit of the LCB. The inner, structurally higher part of the LMSZ consists of green-gray to black, locally gneissic, intensely foliated and lineated amphibolite. Toward the outer or structurally lower part, the amphibolitic rocks grade into gray-green to green, Ep-rich amphibolite, and the intensity of the penetrative fabric progressively decreases. The outer contact is located in concordant intrusions of Hbl-tonalite and/or a mid- to low-T mylonitic narrow band (near Diferencia) or a ductile-brittle fault surface (South of Santiago Rodríguez), which dip a mid- to high-angle to the SW.

The main structural elements of the LMSZ are a syn-metamorphic foliation (S1) and mineral stretching lineation (Le). S1 is defined by the planar alignment of Hbl grains and, locally, by alternating Hbl-rich and Pl-rich segregations (Fig. 4f); Le is defined by elongate Hbl and Pl prismatic grains (Fig. 10d). Regionally, S1 consistently strikes subparallel to the LCB-LMSZ contact and dips at a moderate to high-angle to the SW beneath the plutonic complex (Fig. 8e,k). Le

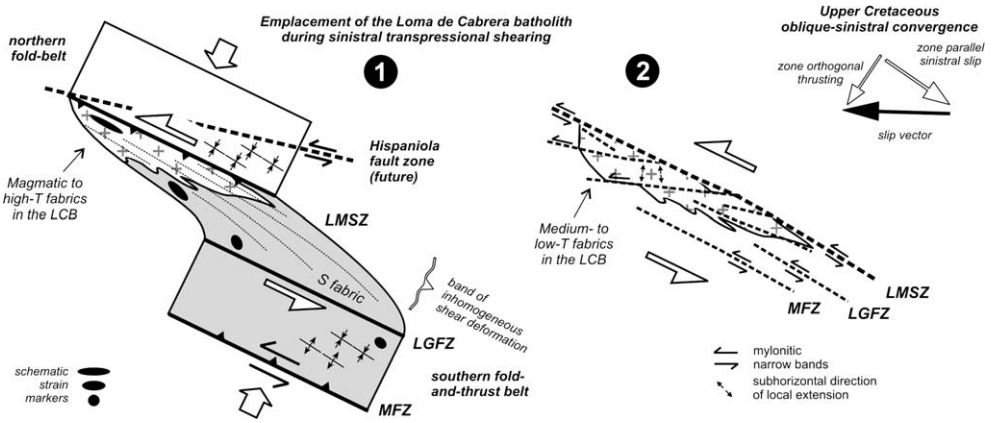

Fig. 11. Schematic diagram showing sinistral strike-slip partitioned transpression in NW Cordillera Central and contemporaneous emplacement of the Loma de Cabrera batholith. During Late Cretaceous oblique-sinistral convergence, the deformation was partitioned between roughly arc-orthogonal pure shear in the northern domain and the southern domain belt and arc-parallel sinistral slip in the La Meseta shear zone (LMSZ). The LCB belongs to an adjacent band of distributed shear deformation. The LMSZ passed westward into a system of W-trending, related minor shear zones that produced local NNW- and SSE-directed extensional movements at the top of the batholith.

commonly plunges at a low angle to the NW or SE (Fig. 8f,l). However, moderate to high angle plunges, down-dip or oblique to S1, are also observed in high strain bands across the lower structural part of the LMSZ (Fig. 8b). This switch in Le orientation probably reflects along-strike variations in finite strain and/or strain partitioning within a transpressive shear zone (Tikoff and Greene, 1997). Mylonitic amphibolites with well-developed asymmetric Hbl and Pl porphyroclasts as well as shear bands were collected for kinematic analysis in several locations of the LMSZ. These kinematic indicators consistently indicate a sinistral strike-slip shear sense parallel to the subhorizontal L1 and top-to-the NW shear sense (i.e. reverse) for the oblique down-dip L1. Consequently, one interpretation of these data is that the LMSZ developed during the oblique thrusting of Cordillera Central over the northern fold-belt. Numerous syn- to late-kinematic Hbl-tonalite dikes occur throughout the LMSZ. The strong magmatic planar fabric and the intrusive contact in the tonalite dikes (Fig. 7e,f) are subparallel to the penetrative S1 fabric in the amphibolites (Fig. 8e,k). Tonalite dikes can be traced into high-shear strain domains, where they are rotated into subparallelism with the regional LMSZ foliation and transformed into L-S mylonitic tectonites (Fig. 4e). These dikes therefore indicate that the amphibolites of the LMSZ formed at least during the syn-kinematic emplacement of the tonalite unit of the LCB.

5. Physical conditions and timing of deformation and plutonism

5.1. Deformation–metamorphism relationships

In the NW Central Cordillera, the mapping of metamorphic facies in metabasic rocks, index mineral occurrences and isograds in metapelitic rocks, reveals a regional NNE-directed metamorphic gradient across the foliation's strike in the southern domain, and a SSW-directed metamorphic gradient in the northern domain (Escuder Viruete, 2004). In both domains, the metamorphic grade increases upward in the structural sequence, from prehnite-pumpellyte facies, through greenschist facies and low-P epidote amphibolite facies, to amphibolite facies, only restricted to LMSZ amphibolites just below the contact with the LCB. Porphyroblast–matrix relationships point to the synchronism of the S1 foliation and peak metamorphism. Therefore, syn-kinematic metamorphic assemblages indicate that temperature increased towards the magmatic axis of the LCB and the adjacent LMSZ. In the amphibolites of the LMSZ, calcic amphiboles parallel to L1 range in composition from Al-tschermakite and tschermakite to Mg-hornblende. Metamorphic temperatures calculated from hornblende-plagioclase rims using the geothermometer of Holland and Blundy (1994) in the lower ($Si_{cat} = 6.9–7.1$ and $Al_T = 1.3–1.6$ for $X_{Ab} = 0.16–0.20$) and upper structural levels ($Si_{cat} = 6.3–6.6$ and $Al_T = 2.3–2.7$ for $X_{Ab} = 0.22–0.28$), demonstrate the upward increase from about 465 to 585 °C in the LMSZ. Furthermore, the sharp decrease in the Al_T content in metamorphic amphiboles between the LMSZ and underlying Duarte Complex suggest a thrust movement and uplift of deep rock along this structure.

5.2. $^{40}Ar/^{39}Ar$ geochronology

5.2.1. Methodology

Selected samples were crushed and sieved to obtain fragments ranging in size from 0.1 to 0.5 mm. A hand magnet was passed over the samples to remove magnetic minerals and metallic crusher fragments/spall. The samples were washed in deionized water, rinsed and then air-dried at room temperature. Mineral separates were hand-picked, wrapped in aluminum foil and stacked in an irradiation capsule with similar-aged samples and neutron flux monitors (Fish Canyon Tuff sanidine, 28.02 Ma; Renne et al., 1998). The samples

were irradiated at the McMaster Nuclear Reactor in Hamilton, Ontario, for 56 MWH, with a neutron flux of approximately 3×10^{16} neutrons/cm^2. Analyses ($n = 54$) of 18 neutron flux monitor positions produced errors of <0.5% in the J value. The mineral separates were step-heated at incrementally higher powers in the defocused beam of a 10 W CO_2 laser (New Wave Research MIR10) until fused, at the Noble Gas Laboratory of the Pacific Centre for Isotopic and Geochemical Research. The gas evolved from each step was analyzed by a VG5400 mass spectrometer equipped with an ion-counting electron multiplier. All measurements were corrected for total system blank, mass spectrometer sensitivity, mass discrimination, radioactive decay during and subsequent to irradiation, as well as interfering Ar from atmospheric contamination and the irradiation of Ca, Cl and K. Isotope production ratios were (^{40}Ar/^{39}Ar)K = 0.0302, (^{37}Ar/^{39}Ar)Ca = 1416.4306, (^{36}Ar/^{39}Ar)Ca = 0.3952, Ca/K = 1.83(^{37}ArCa/^{39}ArK). The plateau and correlation ages of Fig. 12 were calculated using Isoplot 3.09 software (Ludwig, 2003). Errors are quoted at the 2σ (95% confidence) level and are propagated from all sources except mass spectrometer sensitivity and age of the flux monitor. The complete incremental heating ^{40}Ar/^{39}Ar data set for all samples used in this study can be obtained from the electronic supplementary database (Appendix A) or from the first author upon request. The main objective was to obtain geochronological evidence that supports the simultaneity of LCB plutonism and deformation/ metamorphism in the LMSZ.

5.2.2. ^{40}Ar/^{39}Ar samples

Foliated and unfoliated Hbl-tonalites from LCB and LTB and amphibolites with a strong S-L fabric of the LMSZ were selected for dating by ^{40}Ar/^{39}Ar method (Fig. 2 and 12). Sample FC9054-5874II is a coarse-grained isotropic hornblende ± biotite tonalite from the central facies of the LCB in the Loma de Cabrera area. For three steps (3–5), the obtained plateau age from hornblende is 87.9 ± 2.5 Ma (MSWD = 1.01) for 85.6% of the ^{39}Ar released. However, the rock has low potassium content and the majority of gas was released essentially in two steps. No plateau or isochron age was obtained from biotite in this sample, with a disturbed spectrum by possible argon excess. Sample FC9052-5973IV is a hornblende + plagioclase-phyric andesite porphyry that intrudes and cross-cuts the sequence of metabasalts of the Duarte Complex in the Jicomé area. This dike is an apophysis of the LCB in their southern intrusive contact. The sample yielded a plateau age for hornblende of 88.9 ± 2.6 Ma (MSWD = 0.6) for the six high temperature steps (5–10) and 92.9% of the ^{39}Ar released. Inverse isochron age (MSWD = 0.19) is 90.2 ± 7 Ma. Sample JE9083-5874-II is a fine-grained gabbro from Loma Chacuey massif in the Loma de Cabrera area. For seven steps (2–8), the obtained plateau age from hornblende is 83.0 ± 9.2 Ma (MSWD = 1.4) for 97.5% of the ^{39}Ar released. The rock has very low potassium content and very little argon release. Sample MJ9141-5874I is a hornblende-phyric leucotonalite unfoliated dike, intrusive in the metabasalts of the Duarte Complex in the Dajabón area. For six steps (4–10), the obtained hornblende plateau age from hornblende is 83.45 ± 0.83 Ma (MSWD = 0.88) for 94.2% of the ^{39}Ar released. The inverse isochron age (MSWD = 0.38) is 85.0 ± 2.5 Ma. Sample JE9015-5974III is a foliated coarse-grained hornblende ± biotite tonalite from the late batches of magma in the LCB (Santiago Rodríguez area), that intermingles with N70°E mafic dikes in the Río Inaje area. For the four high temperature steps (4–8), the obtained plateau age from hornblende is 73.9 ± 0.48 Ma (MSWD = 1.9) including the 63% of the ^{39}Ar released. In the same rock, the plateau age for biotite is 76.8 ± 0.44 Ma (MSWD = 0.46) for the six high temperature (9–14) steps and 39.2% of the ^{39}Ar released. The inverse isochron age (MSWD = 0.30) is 77.7 ± 1.7 Ma and the integrated age 72.9 ± 0.33 Ma. Sample FC9026-5973IV is a mid- to coarse-grained foliated hornblende tonalite from the LTB in the Jicomé area. The obtained plateau age for hornblende is 74.9 ± 1.8 Ma (MSWD = 0.42) for four steps (3–7) and 89.9% of the ^{39}Ar released. Sample FC9063-5973IV is a blastomylonitic S-L amphibolite from a branch of the LMSZ deforming the Loma Guazumito-Los Charamicos massif in the Jicomé area. The protolith is a low-Ti, island-arc tholeiitic basalt of the Tireo Formation. The obtained hornblende plateau age is 82.8 ± 1.9 Ma (MSWD = 0.46) for all steps (1–9) and 99.99% of the ^{39}Ar released. Inverse isochron age (MSWD = 0.30) is 80.9 ± 3.4 Ma. Sample JE9075-5974III is an amphibolite with a strong S-L fabric from the LMSZ in the Santiago Rodríguez area. Mafic protoliths are basalts of the Duarte Complex. The obtained hornblende plateau age is 74 ± 1.7 Ma (MSWD = 0.95) for four steps (4–7) and 95% of the ^{39}Ar released.

5.2.3. Interpretation

Fig. 13 includes the Ar–Ar ages obtained for this study and other relevant regional data, which permits us to constrain the cooling history of the LCB and the LMSZ. Folding and thrusting of the Tireo Formation in the northern domain took place after 91.8 ± 2.3 Ma and 91.3 ± 2.1 Ma, based on U–Pb dating of extrusion age of arc-related dacite and rhyolite, respectively (Urien et al., 2004). These data are consistent with an Albian to Upper Cenomanian palaeontological age, obtain from foraminifera in cherts of the Tireo Formation near Dajabón by Montgomery and Pessagno (1999). U–Pb zircon analysis of a quartz diorite and hornblende tonalite from the Macutico batholith intrusive in the southern domain, yielded a crystallization age of 90.0 ± 1.9 Ma and 92.1 ± 1.2 Ma, respectively (Joubert et al., 2004). As the geochemical data of arc-related rocks indicate (Escuder Viruete, 2004), dacite and rhyolite of the Tireo Formation are the extrusive equivalent of diorite and tonalite intrusions. On other hand, field evidence indicates that foliated tonalite units of the MB were syn-kinematic with sinistral strike-slip movement along the Macutico fault zone. This, together with the 87.9 ± 1.0 Ma U/Pb zircon ages yielded by the foliated hornblende tonalite intrusive in the LMSZ southeast Diferencia (sample MJ9195-5973I in Fig. 2; Joubert et al., 2004), shows that ductile deformation in the southern domain and sinistral shearing

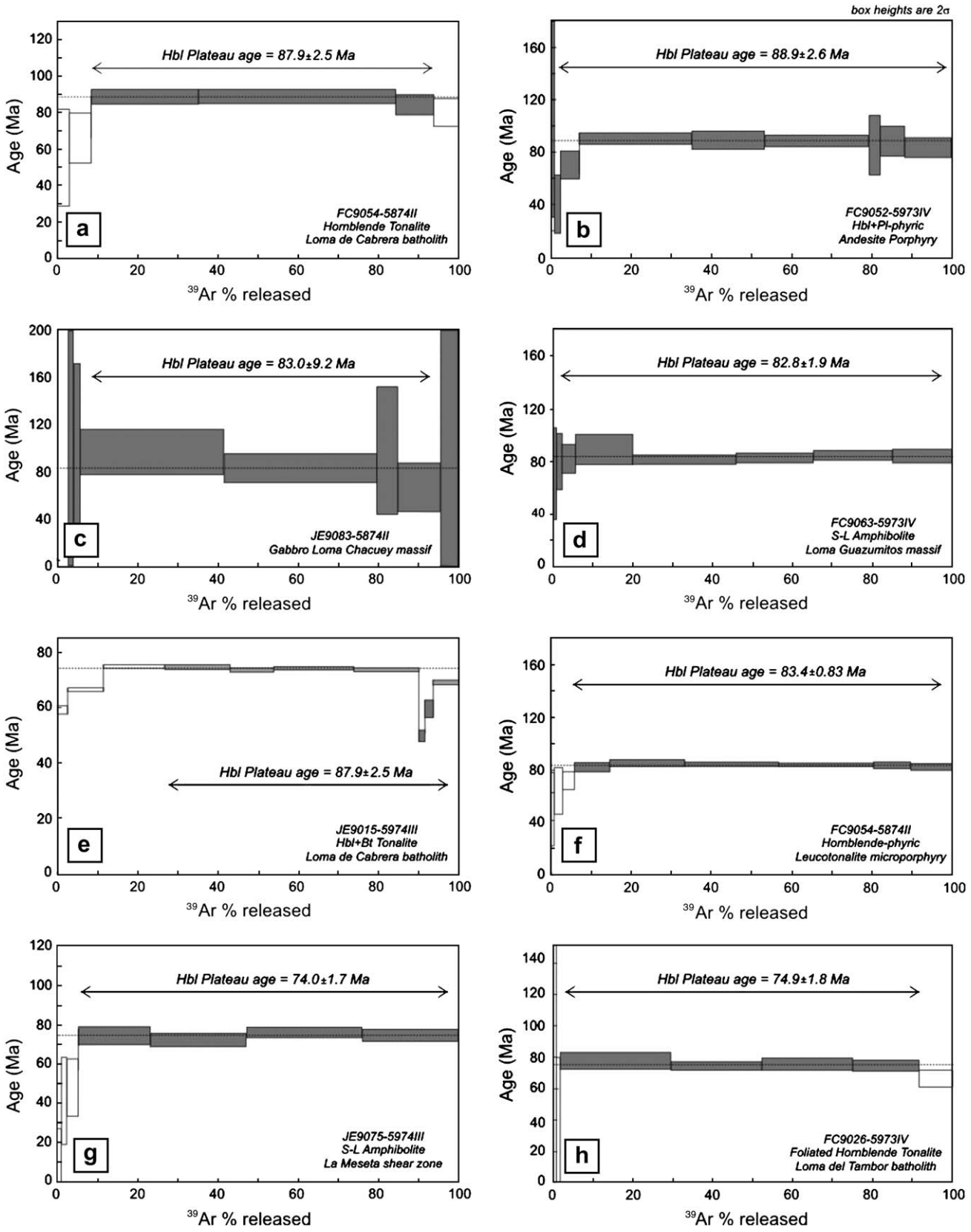

Fig. 12. $^{40}Ar/^{39}Ar$ age spectra for hornblende in samples from the Cordillera Central. The plateau ages were calculated using Isoplot 3.09 software (Ludwig, 2003). Plateau steps are filled, rejected steps are open. Errors are quoted at the 2σ (95% confidence) level and are propagated from all sources except mass spectrometer sensitivity and age of the flux monitor. See text for discussion.

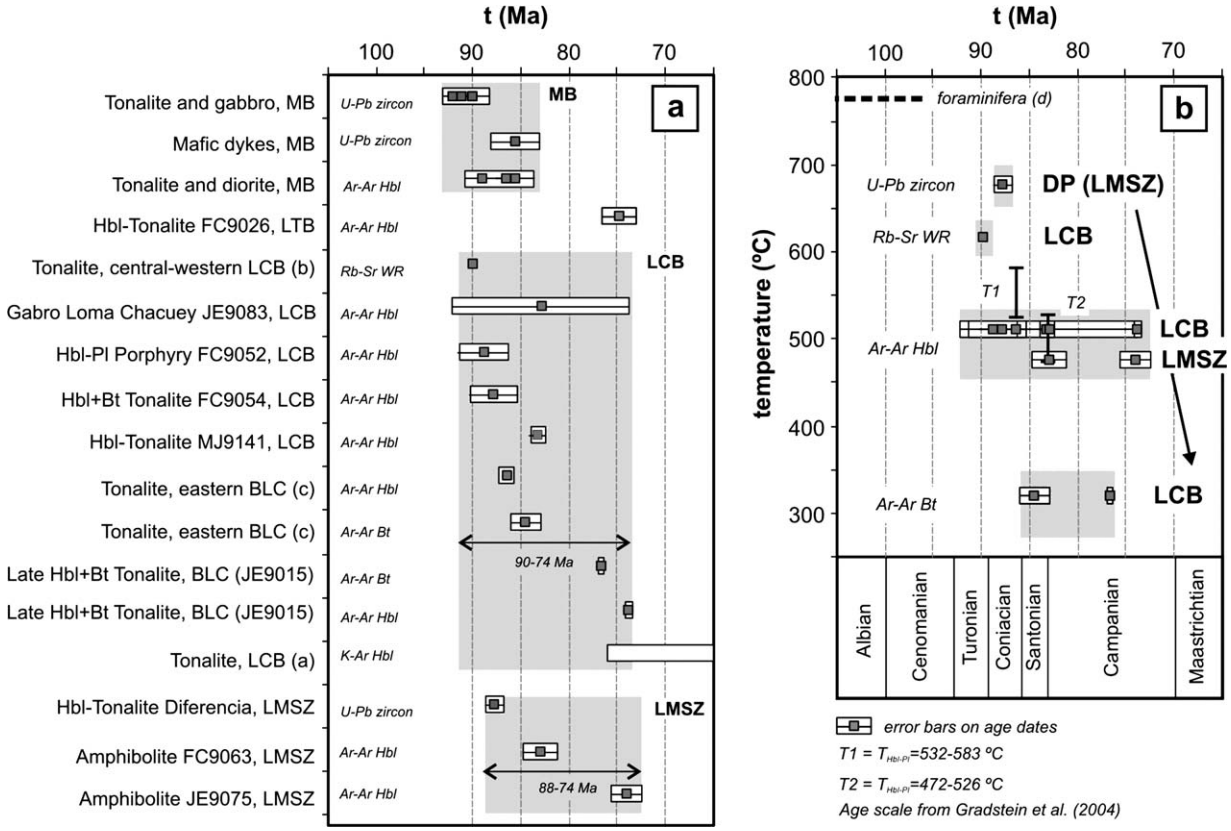

Fig. 13. (a) Summary of geochronological ages for the Loma de Cabrera (LCB), Macutico (MB) and Loma del Tambor (LTB) batholiths and La Meseta shear zone amphibolites (LMSZ). Sources; a, Kesler et al. (1977); b, Feigenson (1978); c, Cribbs et al. (1989); and BGFZ this work. The U-Pb dates of MB and LTB are from Contreras et al. (2004) and Joubert et al. (2004). Rectangles are the error bars (in 2σ). For an Ar closure temperature of hornblende of 525–450 °C and of biotite of 350–260 °C (Dickin, 1995), approximate cooling rates of 50 °C/Ma, 30 °C/Ma and between 50 and 24 °C/km are deduced for Macutico, Loma del Tambor and Loma de Cabrera batholiths, respectively. (b) Cooling history of the Loma de Cabrera batholith and La Meseta shear zone amphibolites, including the U–Pb zircon age of syn-kinematic Hbl-tonalite Diferencia pluton (DP; Joubert et al., 2004). For some rocks, T estimates by Hbl-Pl thermometry are given.

activity along subvertical fault zones was at least from 90 to 88 Ma (Turonian-Coniacian).

The compilation of Rb–Sr whole-rock and ^{40}Ar–^{39}Ar plateau ages of LCB included in Fig. 13a, indicates cooling of the batholith between 90 and 74 Ma. On the basis of these geochronological data, field and microstructural work, ductile deformation along the LMSZ started during the emplacement (88 Ma) of the tonalite units of Diferencia and the LCB, as they cooled through 700–650 °C (Fig. 13b). Deformation continued through Hbl closure at 74 Ma, given the involvement of this mineral in the shearing and evidence for early feldspar plasticity (>500 °C). Hbl-Pl thermobarometric data in amphibolites indicate peak temperatures of 583–472 °C during deformation in the LMSZ (Fig. 13; Escuder Viruete, 2004). Consequently, these results suggest that emplacement of the tonalite of the LCB occurred during sinistral shearing and oblique thrusting in the LMSZ. Although error bars on the Ar–Ar data are large, rapid cooling of the batholith between 90 and 84 Ma (up to 60 °C/Ma) is inferred from Fig. 13b. Then, the batholith and its country rocks appear to have remained ca. 10 Ma in a thermal environment near the Ar–Ar biotite closure temperature (ca. 350 °C), recording late tectonic movements in the LMSZ at 74 Ma.

6. Discussion and conclusions

6.1. Late Cretaceous transpressional shearing in Central Hispaniola

The results above indicate that the NW Cordillera Central area of Hispaniola underwent a heterogeneous ductile deformation in prehnite-pumpellyte and greenschist to amphibolite metamorphic facies conditions during the Late Cretaceous. On a regional scale, this deformation was strongly partitioned in zones of crustal weakness such as subvertical shear/fault zones with serpentinites and thermally softened aureoles around batholiths in the axial area of arc magmatism. Field and geochronological studies indicates that sinistral strike-slip movement acted concurrently with normal shortening across the domain, which is consistent with a transpressional setting for the Late Cretaceous Caribbean magmatic arc (Fig. 14). Evidence for shortening across the region are the subvertical to NE-vergent northern folds with subhorizontal axes, to the north of the LCB and the SW-vergent southern folds and thrusts, to the south of the LCB, both large-scale structures produced by NNE–SSW subhorizontal shortening. Sinistral strike-slip tectonism in the NW Cordillera Central was mainly

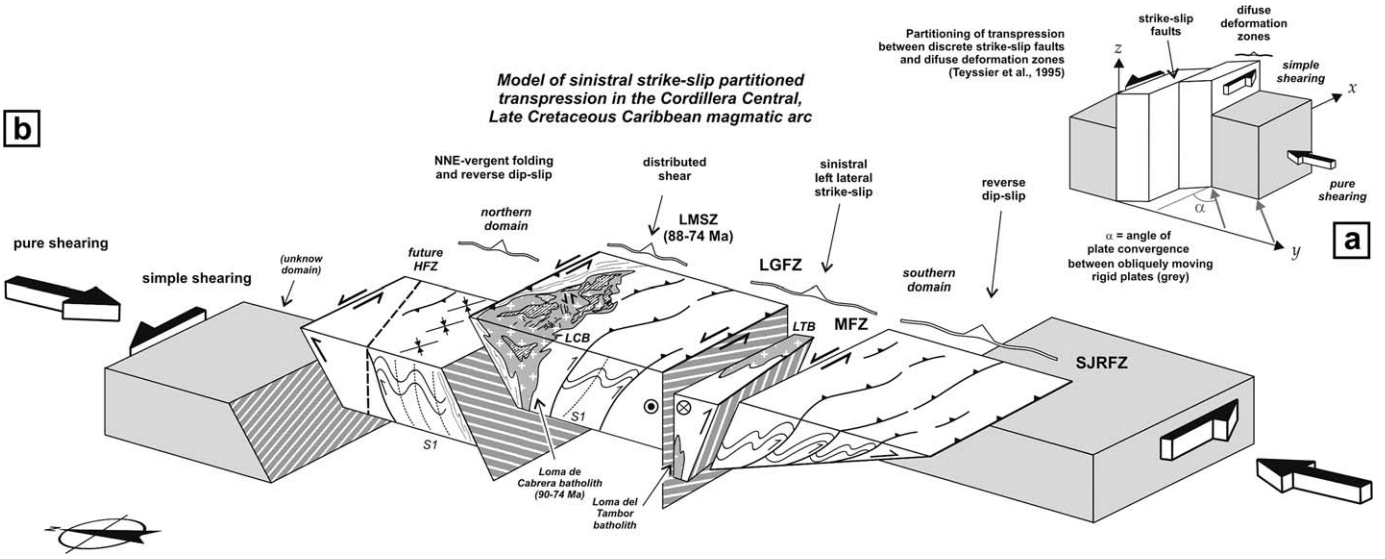

Fig. 14. (a) Kinematic model of partitioned transpression in strike-slip faults and diffuse deformation zones developed between two obliquely converging, rigid plates (Teyssier et al., 1995). (b) Schematic crustal block diagram show the general model for transpressional shearing and strike-slip partitioning during Late Cretaceous deformation in the NW Cordillera Central, Dominican Republic. The structural, petrological and geochronological data argue for the syn-tectonic emplacement and crystallization of the Loma de Cabrera Batholith (90–74 Ma) during sinistral slip along the arc-parallel, crustal scale La Meseta shear zone (at least 88–74 Ma). The arc-orthogonal shortening component of transpression was recorded in the northern and southern domains. The sinistral slip component of transpression is also recorded in the Macutico (MFZ) and La Guácara (LGFZ) fault zones. HFZ, Hispaniola fault zone; SJRFZ, San Juan-Restauración fault zone.

partitioned along the La Meseta shear zone, La Guácara and Macutico fault zones.

Fig. 14 shows a schematic crustal block diagram showing a general model for transpressional shearing and strike-slip partitioning during the Late Cretaceous deformation in the Central Hispaniola. The LCB is elongated subparallel to the WNW–ESE trend of the LMSZ and ductile deformation in the NW Cordillera Central is mainly located in the thermally softened surrounding area, along a deformation zone of related heterogeneously shear (Fig. 14). These two features suggest that contemporaneous, sinistral strike-slip faults focused melts at depth and localized batholiths and regional schistose deformation within higher crustal levels (Hutton, 1988; Clemens and Mawer, 1992; De Saint Blanquat et al., 1998; Chardon, 2003).

The LCB has a general elongated elliptical shape with a long-axis oriented subparallel to the regional structural trend of the Cordillera Central domain. The aspect ratio of the batholith is high (long major axis/minor axis >5) and suggests a low ductility contrast between batholith and country rocks. As previously shown (Brun and Pons, 1981; Castro, 1986), plutons emplaced during regional wrenching have typical strain patterns with sigmoidal foliation trends and slightly plunging stretching lineations, where the internal foliation shows a geometrical continuity with the foliation in the country rocks. This is the case of LCB, where the geometry of the regional strain field is indicated by the batholith orientation and related strain trajectories, which are characterized by a general high-dip WNW–ESE foliation and by a subhorizontal WNW–ESE lineation (Fig. 5). This orientation is consistent with a regional NNE–SSW convergence during intrusion and suggests forceful emplacement of LCB with a subhorizontal direction of expansion parallel to the maximum stretching direction. However, in transpression zones where strike-slip partitioning occurs, the incremental and finite maximum stretching axes are highly oblique with respect to the regional strike-slip shear zones that parallel the magmatic arc trend (Teyssier et al., 1995; De Saint Blanquat et al., 1998; Fossen and Tikoff, 1998). The overall expansion direction of the LCB is $<20^\circ$ with respect to the LMSZ strike, which is compatible with left-oblique convergence.

6.2. Strain intensity patterns and kinematics of deformation

Strain intensity patterns have been successfully used to estimate the relative timing of intrusion and deformation (Brun and Pons, 1981; Hutton, 1988). In the LCB, deformation is heterogeneous and local perturbations in the strain field are related to syntectonic batholith emplacement. Also, finite strain gradients are detected within its country rocks. In the batholith, strain is generally low but increases toward its margins, in particular, along the northern margin. A good example of this increase in strain is given by the microstructural evolution from unfoliated tonalites to solid-state protomylonites and S-C mylonites (Fig. 11). This evolution emphasizes that strain concentrated in the northern, outer part of the pluton during cooling. In the country rocks, strain intensity progressively increases towards the LCB contact. The highest strain intensities occur in the LMSZ amphibolites adjacent to the LCB and decrease outward in the zone of distributed shear. Also, these

characteristics point to the synchronism between LCB emplacement and shearing along the LMSZ (Fig. 14). Strain partitioning of strike-slip deformation in the LCB results mainly from thermal and structural heterogeneities, which are linked to the decrease in T during thermal re-equilibration of tonalites. They give rise to strain localization in marginal zones, i.e. in zones where the temperature drop is expected to be rapid, as the contact with the gabbro-diorite unit and the country rocks. Therefore, the development of strongly foliated tonalites in the LCB marks an increase in strain localization and generally corresponds to the transition from homogeneous weak magmatic fabrics to high- and mid-T solid-state fabrics in the LMSZ system (Fig. 11).

The kinematics of deformation during the emplacement of the LCB has been recognized from shear sense indicators present in magmatic to solid-state deformed tonalites and well developed in zone 3 (Fig. 9). They are related to a combination of ductile sinistral wrenching and oblique thrusting, with local extensional shearing. Sinistral wrench and oblique thrusting components are mainly detected: (i) near the NE contact of LCB with the LMSZ amphibolites, where strongly foliated tonalites and S-C orthogenesis occur; and (ii) within localized internal WNW–ESE to W–E trending, high-dip shear zones related with the LMSZ system. Top-to-the N and NW reverse shear-sense observed in south dipping S-L amphibolites of the LMSZ, could be explained by syn-emplacement oblique thrusting of the LCB. Extensional shears occur near the roof of the LCB, around Lomas Altas, Cerro del Pescado and Loma Guazumito-Los Charamicos gabbro-ultramafic massifs (Fig. 9), where oblique top-to-the N and S movements in low-dip foliations indicate a combination of dominant dip-slip and strike-slip displacements. Generally, they are associated with the mid- to low-T solid-state deformation marked by the development of heterogeneous S-C shear bands. Zones of opposite sense of shear around the gabbro-ultramafic massifs can be related both to doming effects related to batholith emplacement, gravity collapse of roof wall, or a local N–S extension effect linked to the sinistral transpressive regional tectonics (Fig. 11). The late dike swarm emplacement occurred in steeply dipping, planar fracture conduits oriented oblique to the LCB trend and regional structure (Fig. 7d,g,h). They can be related to an arc-parallel, sinistral strike-slip component that produced W–E trending tension fractures due to an oblique convergence direction.

6.3. Syntectonic emplacement of the Loma de Cabrera batholith

Syntectonic metamorphism is observed in the amphibolites of the LMSZ, mainly produced by heat loss from the tonalitic magma. Synchronism between LCB emplacement and metamorphism in the LMSZ is demonstrated by the following characteristics: (i) metamorphic assemblages indicate

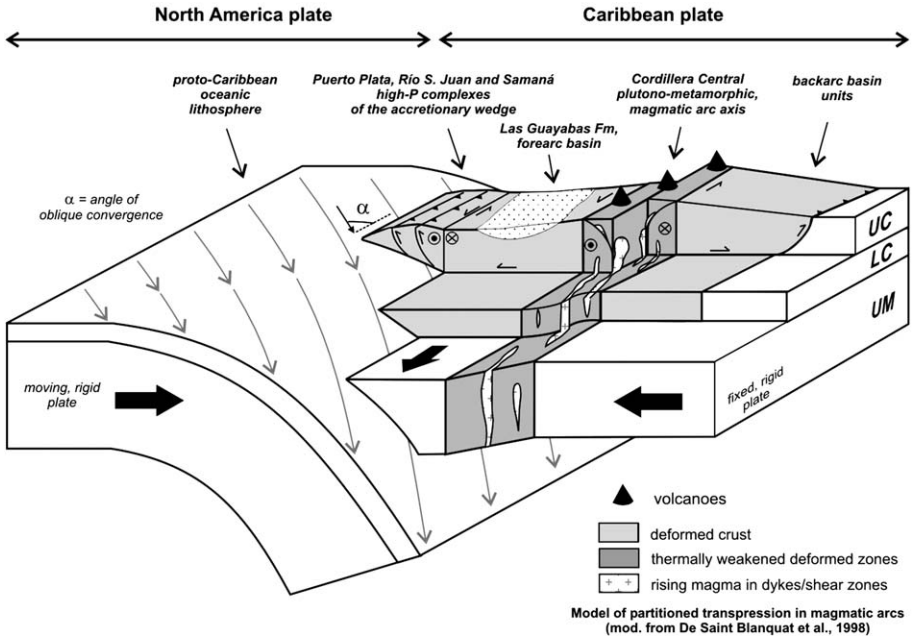

Fig. 15. 3-D model of transpressional geometry and kinematics in magmatic arcs (De Saint Blanquat et al., 1998) applied to the Late Cretaceous Caribbean island-arc in the Hispaniola segment. Oblique motion imposed by the subducting Atlantic oceanic lithosphere is transferred to the relatively fixed Caribbean oceanic lithosphere through the "strong" upper mantle. Vertical coupling between strike-slip partitioning and distributed shearing in the arc upper crust and localized shearing in the upper mantle is provided by distributed shearing in the lower crust. This causes the parallelism of opposite-vergent structures in the forearc and backarc regions. Transpressional systems are preferentially intruded by magmas because of the steep pressure gradients in subvertical strike-slip shear zones and their ability to force magma upward. A Caribbean example is the Loma de Cabrera batholith intruded along the La Meseta shear zone. FMS, forearc mantle sliver that undergoes margin-parallel translation.

temperature increase towards batholith; (ii) amphibole nematoblasts grew syn-kinematic to the S1-L1 fabric and show a core-to-rim chemical zoning that recorded growth during increasing P and T (Escuder Viruete, 2004); (iii) S-C fabrics and sigmoidal inclusion trails in plagioclase and Al-tschemarkite define a shear sense consistent with the regional sinistral wrenching and oblique thrusting; and (iv) Ar–Ar dating shows that hornblende in amphibolite and in tonalite are comparable in age.

Finite strain is greater in the LMSZ than in the northern and the southern domains. This indicates that the LMSZ system and the LCB emplacement favored the strike-slip component of transpression over normal shortening in the rest of NW Cordillera Central area. Given their arc-parallel geometry, strike-slip systems tend to favor plutonic activity as they provide deep crustal-scale vertical pressure gradients (Fig. 15; De Saint Blanquat et al., 1998). For any angle of oblique convergence, magma-assisted strike-slip can also be enabled by the intrusion of batholiths. In this sense, Fig. 15 shows a 3-D model of transpressional geometry and kinematics in the Late Cretaceous for the Hispaniola segment of the Caribbean island-arc, and the probable organization in the regions of forearc and backarc. In the present case, slip along the LMSZ was probably active slightly before LCB emplacement, suggesting that strike-slip partitioning facilitated magma ascent. Later deformations in Eocene to Recent times are evidenced by the HFZ, which cuts the LCB macrostructure obliquely, and by variable reactivation of shear and thrust fault zones under brittle conditions.

Acknowledgements

This work forms part of the geothematic cartographic project of the Dominican Republic financed by the SYSMIN program (EU) and also received financial aid from MCYT projects BTE-2002-00326 and CGL2005-02162/BTE. John F. Lewis (George Washington University) and Gren Draper (Florida International University) are thanked for their introduction to the area, initial field-work and continued discussions and advice on the Caribbean arc-related igneous rocks in general, and the Loma de Cabrera batholith in particular. We also express our thanks to D. Brown and J.F. Lewis for careful reviews of the manuscript.

Appendix A. Incremental heating $^{40}Ar/^{39}Ar$ data for hornblende and biotite, NW Cordillera Central, Dominican Republic

Power (%)	$^{40}Ar/^{39}Ar$	$^{38}Ar/^{39}Ar$	$^{37}Ar/^{39}Ar$	$^{36}Ar/^{39}Ar$	Ca/K	Cl/K	% $^{40}Ar_{atm}$	f ^{39}Ar	$^{40}Ar^*/^{39}ArK$	Age
FC 9054 5874-II hornblende										
2.1	65.918 ± 0.036	0.325 ± 0.083	1.419 ± 0.057	0.210 ± 0.043	5.393	0.062	92.48	2.77	4.581 ± 2.221	55.43 ± 26.46
2.4	27.954 ± 0.023	0.700 ± 0.115	2.874 ± 0.030	0.078 ± 0.045	11.127	0.155	78.45	5.44	5.488 ± 1.147	66.20 ± 13.59
2.7	11.270 ± 0.030	2.845 ± 0.072	6.393 ± 0.033	0.017 ± 0.037	24.985	0.655	31.76	26.81	7.402 ± 0.337	88.74 ± 3.94
3	10.221 ± 0.020	3.735 ± 0.022	7.292 ± 0.023	0.015 ± 0.066	28.546	0.862	26.27	49.29	7.404 ± 0.334	88.76 ± 3.90
3.3	12.409 ± 0.019	3.012 ± 0.059	6.707 ± 0.022	0.023 ± 0.067	26.223	0.694	36.32	9.5	7.030 ± 0.469	84.38 ± 5.50
4	13.366 ± 0.010	2.571 ± 0.048	6.918 ± 0.016	0.027 ± 0.078	27.055	0.592	40.61	6.19	6.660 ± 0.643	80.03 ± 7.56
Tot/Av.	12.622 ± 0.006	3.083 ± 0.011	13.895 ± 0.005	0.023 ± 0.014		0.503		100	7.362 ± 0.107	85.65 ± 1.26
$J = 0.006811 \pm 0.000018$; volume $^{39}ArK = 121.41$; integrated date = 85.65 ± 2.53; plateau age = 87.9 ± 2.5										
FC 9052 5973-IV hornblende										
2.1	309.447 ± 0.022	0.681 ± 0.090	2.864 ± 0.049	1.070 ± 0.050	10.087	0.111	98.6	0.29	3.882 ± 15.157	47.68 ± 183.70
2.4	231.761 ± 0.044	0.242 ± 0.105	2.135 ± 0.045	0.764 ± 0.053	7.641	0.02	94.64	0.79	11.791 ± 9.822	141.07 ± 113.04
2.7	74.072 ± 0.031	0.180 ± 0.126	2.841 ± 0.042	0.249 ± 0.034	10.328	0.028	95.01	1.44	3.300 ± 1.822	40.60 ± 22.17
3	30.808 ± 0.036	0.674 ± 0.094	9.161 ± 0.040	0.093 ± 0.037	33.894	0.15	79.8	4.6	5.781 ± 0.895	70.54 ± 10.71
3.3	13.339 ± 0.023	1.110 ± 0.034	13.059 ± 0.026	0.028 ± 0.033	48.576	0.255	43.3	28.21	7.461 ± 0.346	90.54 ± 4.09
3.5	15.662 ± 0.028	1.017 ± 0.103	13.220 ± 0.032	0.037 ± 0.050	49.196	0.233	51.8	17.98	7.369 ± 0.591	89.45 ± 6.99
3.7	13.069 ± 0.023	0.993 ± 0.082	14.304 ± 0.029	0.028 ± 0.041	52.736	0.228	43.14	26.58	7.322 ± 0.393	88.90 ± 4.65
3.9	75.221 ± 0.019	0.634 ± 0.068	14.421 ± 0.023	0.247 ± 0.034	53.253	0.135	91.26	2.81	6.342 ± 2.632	77.25 ± 31.38
4.2	27.851 ± 0.022	0.791 ± 0.052	14.637 ± 0.024	0.080 ± 0.041	54.019	0.178	72.33	6.03	7.320 ± 0.989	88.87 ± 11.71
4.5	19.221 ± 0.013	1.123 ± 0.087	13.625 ± 0.018	0.051 ± 0.039	50.194	0.257	62.66	11.27	6.916 ± 0.606	84.07 ± 7.20
Tot/Av.	20.175 ± 0.005	0.985 ± 0.017	26.150 ± 0.005	0.052 ± 0.008		0.159		100	7.294 ± 0.120	87.35 ± 1.43
$J = 0.006898 \pm 0.000020$; volume $^{39}ArK = 202.3$; integrated date = 87.35 ± 2.86; plateau age = 88.9 ± 2.6										
JE 9083 5874-II hornblende										
1.8	120.759 ± 0.060	1.362 ± 0.123	4.176 ± 0.090	0.290 ± 0.153	19.928	0.309	80.05	2.53	21.874 ± 12.609	249.11 ± 134.12
2	222.513 ± 0.067	0.441 ± 0.291	13.154 ± 0.084	0.643 ± 0.136	69.711	0.088	98.42	1.13	3.201 ± 24.298	38.67 ± 290.44
2.3	145.368 ± 0.431	0.493 ± 0.316	13.564 ± 0.080	0.234 ± 0.309	75.587	0.113	53.96	1.8	61.156 ± 68.732	624.93 ± 593.61
2.6	19.368 ± 0.010	1.335 ± 0.179	12.890 ± 0.015	0.047 ± 0.114	76.728	0.31	57.37	36.02	8.082 ± 1.649	96.09 ± 19.09
2.9	16.445 ± 0.019	1.500 ± 0.055	11.983 ± 0.023	0.041 ± 0.087	71.174	0.349	56.84	38.56	6.891 ± 1.070	82.25 ± 12.49
3.2	34.003 ± 0.038	1.801 ± 0.076	14.528 ± 0.044	0.075 ± 0.205	85.193	0.425	70.94	5.12	8.230 ± 4.739	97.81 ± 54.82
3.6	22.890 ± 0.025	1.334 ± 0.109	16.664 ± 0.031	0.062 ± 0.094	99.549	0.314	72.99	10.8	5.524 ± 1.780	66.23 ± 20.95
4.2	33.604 ± 0.036	1.177 ± 0.077	43.268 ± 0.040	0.092 ± 0.347	276.848	0.296	67.54	4.05	9.082 ± 10.489	107.64 ± 120.68
Tot/Av.	24.572 ± 0.023	1.394 ± 0.034	44.175 ± 0.005	0.067 ± 0.026		0.275		100	6.748 ± 0.788	

Appendix A (*continued*)

Power (%)	$^{40}Ar/^{39}Ar$	$^{38}Ar/^{39}Ar$	$^{37}Ar/^{39}Ar$	$^{36}Ar/^{39}Ar$	Ca/K	Cl/K	% $^{40}Ar_{atm}$	f ^{39}Ar	$^{40}Ar^*/^{39}ArK$	Age
$J = 0.006769 \pm 0.000018$; volume $^{39}ArK = 10.98$; integrated date $= 102.66 \pm 18.18$; plateau age $= 83 \pm 9.2$										
FC 9063 5973-IV hornblende										
1.8	265.285 ± 0.093	0.358 ± 0.279	2.363 ± 0.111	0.908 ± 0.141	8.82	0.053	99.99	0.08	−0.006 ± 28.788	−0.07 ± 352.35
2.1	47.919 ± 0.019	0.328 ± 0.045	2.367 ± 0.025	0.146 ± 0.069	12.57	0.068	86.45	0.62	5.840 ± 2.957	70.09 ± 34.81
2.4	28.515 ± 0.023	0.354 ± 0.102	4.247 ± 0.031	0.079 ± 0.077	23.407	0.076	75.01	1.47	6.659 ± 1.815	79.71 ± 21.25
2.7	17.580 ± 0.021	1.875 ± 0.038	6.095 ± 0.025	0.043 ± 0.072	33.976	0.43	59.73	3.48	6.810 ± 0.945	81.48 ± 11.05
3	11.207 ± 0.086	4.586 ± 0.185	6.434 ± 0.022	0.019 ± 0.048	35.99	1.062	33.58	14.49	7.402 ± 1.012	88.39 ± 11.80
3.3	8.556 ± 0.027	5.646 ± 0.047	6.677 ± 0.026	0.013 ± 0.063	37.388	1.309	20.51	25.79	6.798 ± 0.322	81.34 ± 3.77
3.6	8.842 ± 0.028	7.097 ± 0.135	7.832 ± 0.028	0.015 ± 0.042	43.968	1.651	22.32	19.4	6.856 ± 0.286	82.01 ± 3.35
3.9	9.022 ± 0.028	6.594 ± 0.129	8.747 ± 0.025	0.015 ± 0.039	49.212	1.537	21.81	19.91	7.061 ± 0.291	84.42 ± 3.40
4.4	9.759 ± 0.029	7.245 ± 0.039	9.020 ± 0.028	0.018 ± 0.072	50.782	1.69	28.02	14.75	7.006 ± 0.466	83.77 ± 5.45
Tot/Av.	10.084 ± 0.009	5.926 ± 0.025	22.729 ± 0.004	0.017 ± 0.012		0.875		100	6.991 ± 0.103	83.31 ± 1.21
$J = 0.006784 \pm 0.000018$; volume $^{39}ArK = 200.13$; integrated date $= 83.31 \pm 2.43$; plateau age $= 82.8 \pm 1.9$										
JE 9015 5974-II hornblende (possible biotite inclusions)										
2	14.303 ± 0.012	0.099 ± 0.010	0.002 ± 2.663	0.036 ± 0.010	0.014	0.018	74.09	3.31	3.688 ± 0.092	59.00 ± 1.44
2.3	6.944 ± 0.007	0.031 ± 0.006	−0.001 ± 1.997	0.010 ± 0.006	0	0.004	39.82	9.05	4.162 ± 0.037	66.44 ± 0.58
2.5	7.430 ± 0.008	0.032 ± 0.007	0.007 ± 0.276	0.009 ± 0.007	0.062	0.004	36.75	7.33	4.685 ± 0.044	74.61 ± 0.69
2.8	7.581 ± 0.007	0.047 ± 0.007	0.011 ± 1.172	0.010 ± 0.007	0.092	0.007	38	7.81	4.685 ± 0.043	74.62 ± 0.68
3.1	6.813 ± 0.009	0.231 ± 0.016	0.066 ± 0.844	0.007 ± 0.007	0.568	0.05	31.09	16.28	4.681 ± 0.054	74.55 ± 0.85
3.3	7.879 ± 0.006	0.233 ± 0.008	0.032 ± 2.722	0.011 ± 0.005	0.281	0.05	41.22	10.72	4.617 ± 0.040	73.56 ± 0.62
3.5	7.118 ± 0.006	0.325 ± 0.012	0.127 ± 0.490	0.009 ± 0.005	1.1	0.071	34.43	19.92	4.655 ± 0.032	74.14 ± 0.51
3.7	7.255 ± 0.006	0.319 ± 0.011	0.021 ± 2.193	0.009 ± 0.005	0.178	0.069	36.13	16.1	4.619 ± 0.037	73.59 ± 0.58
3.9	21.560 ± 0.014	0.260 ± 0.013	0.005 ± 7.490	0.063 ± 0.013	0.046	0.054	85.52	1.36	3.102 ± 0.128	49.74 ± 2.02
4.4	14.516 ± 0.021	0.247 ± 0.037	0.018 ± 3.805	0.037 ± 0.016	0.157	0.052	74.26	2.09	3.719 ± 0.204	59.48 ± 3.21
5	8.849 0.009	0.235 ± 0.015	0.090 ± 0.293	0.016 ± 0.009	0.775	0.05	50.97	6.05	4.324 ± 0.052	68.98 ± 0.82
Tot/Av.	7.934 ± 0.001	0.213 ± 0.003	0.237 ± 0.042	0.012 ± 0.001		0.039		100	4.654 ± 0.011	71.99 ± 0.22
$J = 0.009013 \pm 0.000034$; volume $^{39}ArK = 0.12$; integrated date $= 71.99 \pm 0.43$; plateau age $= 73.9 \pm 0.48$										
JE 9015 5974-II biotite										
2	17.100 ± 0.005	0.043 ± 0.004	0.006 ± 0.285	0.057 ± 0.004	0.055	0.004	96.13	0.92	0.633 ± 0.081	10.26 ± 1.30
2.2	8.318 ± 0.008	0.032 ± 0.006	0.001 ± 0.599	0.020 ± 0.006	0.01	0.003	71.6	3.61	2.340 ± 0.051	37.65 ± 0.80
2.4	6.207 ± 0.006	0.027 ± 0.014	0.000 ± 1.665	0.008 ± 0.005	0.002	0.003	37.73	11.67	3.848 ± 0.028	61.50 ± 0.44
2.5	5.714 ± 0.007	0.026 ± 0.020	0.000 ± 1.598	0.004 ± 0.006	0.002	0.003	17.99	7.91	4.671 ± 0.036	74.39 ± 0.55
2.6	5.584 ± 0.006	0.025 ± 0.012	0.000 ± 1.090	0.003 ± 0.005	0.003	0.002	16.72	14.32	4.636 ± 0.031	73.84 ± 0.49
2.7	5.592 ± 0.007	0.026 ± 0.015	0.001 ± 0.470	0.002 ± 0.006	0.006	0.003	10.35	11.04	5.000 ± 0.034	79.51 ± 0.54
2.8	5.921 ± 0.015	0.026 ± 0.027	0.000 ± 0.856	0.003 ± 0.013	0.004	0.003	15.53	6.32	4.988 ± 0.082	79.32 ± 1.28
2.9	5.890 ± 0.007	0.026 ± 0.031	0.002 ± 0.499	0.003 ± 0.006	0.015	0.003	15.87	4.97	4.942 ± 0.037	78.60 ± 0.58
3.1	5.685 ± 0.006	0.027 ± 0.019	0.000 ± 3.995	0.003 ± 0.005	0.002	0.003	14.9	8.23	4.824 ± 0.030	76.77 ± 0.46
3.3	5.687 ± 0.008	0.028 ± 0.020	0.002 ± 0.999	0.003 ± 0.007	0.017	0.003	14.76	7.61	4.834 ± 0.044	76.92 ± 0.68
3.5	5.878 ± 0.006	0.031 ± 0.027	0.001 ± 1.498	0.004 ± 0.006	0.006	0.004	17.9	4.97	4.811 ± 0.031	76.57 ± 0.49
3.8	5.699 ± 0.007	0.030 ± 0.023	0.007 ± 0.490	0.003 ± 0.007	0.062	0.004	15.27	5.99	4.814 ± 0.037	76.63 ± 0.57
4.4	5.661 ± 0.005	0.029 ± 0.025	0.002 ± 1.748	0.003 ± 0.005	0.015	0.003	14.28	5.74	4.838 ± 0.027	77.00 ± 0.42
5.5	5.534 ± 0.006	0.026 ± 0.023	0.008 ± 0.495	0.002 ± 0.004	0.068	0.003	12.5	6.69	4.829 ± 0.035	76.85 ± 0.54
Tot/Av.	5.967 ± 0.001	0.027 ± 0.003	0.008 ± 0.027	0.005 ± 0.001		0.003		100	4.826 ± 0.007	72.95 ± 0.17
$J = 0.009012 \pm 0.000032$; volume $^{39}ArK = 0.5$; integrated date $= 72.95 \pm 0.33$; plateau age $= 76.8 \pm 0.44$										
JE 9075 5974-III hornblende										
1.8	52.995 ± 0.349	0.309 ± 0.373	0.618 ± 0.365	0.347 ± 0.391	2.562	0.056	206.91	0.49	−48.278 ± 23.054	−714.66 ± 418.75
2.1	81.945 ± 0.033	0.680 ± 0.133	3.340 ± 0.042	0.294 ± 0.065	17.28	0.144	104.51	0.35	−3.243 ± 5.279	−40.08 ± 65.97
2.4	32.548 ± 0.025	0.222 ± 0.075	4.945 ± 0.034	0.104 ± 0.063	26.911	0.045	88.53	1.13	3.355 ± 1.861	40.55 ± 22.24
2.8	19.396 ± 0.016	0.565 ± 0.086	8.298 ± 0.021	0.060 ± 0.069	46.016	0.126	78.55	3.07	3.944 ± 1.239	47.57 ± 14.76
3.2	9.217 ± 0.032	1.237 ± 0.054	9.360 ± 0.028	0.019 ± 0.051	52.183	0.285	32.85	18.1	6.160 ± 0.382	73.76 ± 4.48
3.5	8.776 ± 0.022	1.321 ± 0.033	9.794 ± 0.017	0.018 ± 0.044	54.665	0.305	31.89	24.06	5.983 ± 0.304	71.69 ± 3.58
3.8	8.895 ± 0.012	1.239 ± 0.076	10.568 ± 0.017	0.018 ± 0.040	59.089	0.286	29.51	28.99	6.310 ± 0.240	75.52 ± 2.82
4.1	8.896 ± 0.020	1.312 ± 0.106	10.842 ± 0.016	0.019 ± 0.033	60.65	0.304	30.74	23.82	6.182 ± 0.255	74.02 ± 2.99
Tot/Av.	9.707 ± 0.005	1.232 ± 0.019	29.924 ± 0.003	0.022 ± 0.012		0.194		100	6.166 ± 0.086	69.08 ± 1.01
$J = 0.006775 \pm 0.000018$; volume $^{39}ArK = 157.49$; integrated date $= 69.08 \pm 2.03$; plateau age $= 74 \pm 1.7$										
FC 9026 5973-4 hornblende										
2.1	128.211 ± 0.030	1.048 ± 0.090	2.681 ± 0.051	0.369 ± 0.041	10.508	0.221	77.84	0.67	24.505 ± 3.471	281.87 ± 36.97
2.3	77.676 ± 0.022	0.277 ± 0.121	2.627 ± 0.033	0.269 ± 0.061	10.354	0.048	97.01	0.93	1.910 ± 4.559	23.62 ± 56.02
2.6	10.596 ± 0.051	0.633 ± 0.045	9.151 ± 0.047	0.021 ± 0.052	37.004	0.143	38.11	27.7	6.358 ± 0.451	77.47 ± 5.38
2.9	9.898 ± 0.019	0.781 ± 0.031	8.598 ± 0.021	0.019 ± 0.028	34.738	0.177	35.59	22.8	6.091 ± 0.221	74.28 ± 2.65
3.1	10.973 ± 0.030	0.757 ± 0.047	8.336 ± 0.034	0.022 ± 0.039	33.667	0.171	41.25	22.65	6.191 ± 0.332	75.48 ± 3.97
3.3	12.129 ± 0.012	0.779 ± 0.024	8.502 ± 0.019	0.027 ± 0.033	34.343	0.176	46.91	16.74	6.111 ± 0.283	74.52 ± 3.38
4	14.180 ± 0.032	0.721 ± 0.054	8.508 ± 0.034	0.036 ± 0.036	34.364	0.163	57.82	8.49	5.415 ± 0.434	66.19 ± 5.21
Tot/Av.	11.664 ± 0.008	0.722 ± 0.010	18.674 ± 0.007	0.024 ± 0.010		0.157		100	6.158 ± 0.085	75.81 ± 1.02

(*continued on next page*)

Appendix A (*continued*)

Power (%)	$^{40}Ar/^{39}Ar$	$^{38}Ar/^{39}Ar$	$^{37}Ar/^{39}Ar$	$^{36}Ar/^{39}Ar$	Ca/K	Cl/K	% $^{40}Ar_{atm}$	f ^{39}Ar	$^{40}Ar^*/^{39}ArK$	Age
$J = 0.006901 \pm 0.000020$; volume $^{39}ArK = 243.33$; integrated date $= 75.81 \pm 2.04$; plateau age $= 74.9 \pm 1.8$										
MJ 9141 5874-I hornblende										
2.1	520.731 ± 0.033	0.363 ± 0.183	1.343 ± 0.084	1.827 ± 0.053	4.02	0.002	100.6	0.07	-2.941 ± 26.328	-36.96 ± 334.27
2.4	69.989 ± 0.028	0.115 ± 0.091	1.996 ± 0.035	0.231 ± 0.041	7.153	0.013	93.66	0.67	4.028 ± 2.304	49.42 ± 27.88
2.7	40.422 ± 0.021	0.100 ± 0.074	2.898 ± 0.026	0.124 ± 0.041	10.493	0.015	86.46	2.1	5.202 ± 1.494	63.57 ± 17.95
2.9	19.384 ± 0.021	0.154 ± 0.070	3.885 ± 0.025	0.049 ± 0.037	14.1	0.03	67.35	2.93	5.860 ± 0.572	71.46 ± 6.84
3.1	11.820 ± 0.018	0.167 ± 0.117	4.178 ± 0.018	0.020 ± 0.037	15.179	0.034	41.03	9.1	6.717 ± 0.281	81.67 ± 3.34
3.6	9.606 ± 0.016	0.160 ± 0.117	4.177 ± 0.021	0.012 ± 0.043	15.175	0.033	25.83	18.62	6.984 ± 0.201	84.85 ± 2.39
3.5	9.000 ± 0.011	0.155 ± 0.084	4.262 ± 0.019	0.010 ± 0.036	15.489	0.032	22	23.74	6.910 ± 0.131	83.97 ± 1.56
3.7	8.955 ± 0.009	0.150 ± 0.046	4.171 ± 0.016	0.010 ± 0.027	15.154	0.031	22.1	23.86	6.866 ± 0.107	83.44 ± 1.27
3.9	11.763 ± 0.015	0.153 ± 0.039	4.029 ± 0.020	0.020 ± 0.028	14.633	0.031	39.84	9.18	6.819 ± 0.218	82.88 ± 2.60
4.2	11.576 ± 0.014	0.150 ± 0.043	3.932 ± 0.017	0.019 ± 0.035	14.279	0.031	39.68	9.73	6.738 ± 0.230	81.93 ± 2.73
Tot/Av.	11.216 ± 0.003	0.153 ± 0.017	8.104 ± 0.003	0.017 ± 0.007		0.025		100	6.868 ± 0.041	82.39 ± 0.50
$J = 0.006895 \pm 0.000020$; volume $^{39}ArK = 536.47$; integrated date $= 82.39 \pm 1.00$; plateau age $= 83.45 \pm 0.83$ Ma										

Volumes are 1E−13 cm^3 NPT. Age uncertainties are reported at the 2σ level.

References

Bellier, O., Sebrier, M., 1994. Relationship between tectonic and volcanism along the Great Sumatran Fault Zone deduced by SPOT image analyses. Tectonophysics 233, 215–231.

Bowin, C., 1975. The geology of Española. In: Naim, A., Stehli, F. (Eds.), The Ocean Basins and Margins: The Gulf of Mexico and the Caribbean, Vol. 3. Plenum Press, New York, pp. 501–552.

Brown, M., D'Lemos, R.S., 1991. The Cadomian granites of Mancellia, northeast Armorican Massif of France: relationship to the St. Maló migmatitic belt, petrogenesis and tectonic setting. Precambrian Research 51, 393–427.

Brun, P., Pons, J., 1981. Strain patterns of pluton emplacement in a crust undergoing non-coaxial deformation, Sierra Morena, Southern Spain. Journal of Structural Geology 3, 219–229.

Chardon, D., 2003. Strain partitioning and batholith emplacement at the roof of a transpressive magmatic arc. Journal of Structural Geology 25, 91–107.

Castro, A., 1986. Structural pattern and ascent model in the Central Extremadura batholith, Hercynian belt, Spain. Journal of Structural Geology 8, 633–645.

Chemenda, A., Lallemand, S., Bokun, A., 2000. Strain partitioning and interplate friction in oblique subduction zones: Constraints provided by experimental modeling. Journal of Geophysical Research 105 (B3), 5567–5581.

Clemens, J.D., Mawer, C.K., 1992. Granite magma transport by fracture propagation. Tectonophysics 6, 343–361.

Contreras, F., Ardévol, Ll, Granados, L., Calvo, J.P., Escuder Viruete, J., Escuer, J., Florido, P., Antón Pacheco, C., García Lobón, J.L., Mortensen, J.K., Ullrich, T., Friedman, R., 2004. Mapa Geológico de la República Dominicana E. 1:50.000, Jicomé (5973-IV). Dirección General de Minería, Santo Domingo, 158 pp.

Crawford, W.A., Crawford, M.L., 1991. Magma emplacement in a convergent tectonic orogen, southern Revillagigedo Island, southeastern Alaska. Canadian Journal of Earth Sciences 28, 929–938.

Cribb, T.W., 1986. The petrology and geochemistry of eastern Loma de Cabrera batholith. The George Washington University, MSc thesis, 122 pp.

Cribb, J.W., Jimenez, J., Lewis, J.F., Sutter, J.F., 1989. $^{40}Ar/^{39}Ar$ ages from Loma de Cabrera batholith: implications for timing of tectonic events in northern Hispaniola. Geological Society of American Abstracts with Programs 21 (6), A267.

Draper, G., Lewis, J., 1991. Metamorphic belts in Central Española. In: Mann, P., Draper, G., Lewis, J.F. (Eds.), Geologic and Tectonic Development of the North America-Caribbean Plate Boundary in Española, 262. Geological Society of America Special Paper, pp. 29–46.

De Saint Blanquat, M., Tikoff, B.T., Teyssier, C., Vigneresse, J.L., 1998. Transpressional kinematics and magmatic arcs. In: Holdsworth, R.E., Strachan, R.A., Dewey, J.F. (Eds.), Continental Transpressional and Transtensional Tectonics, 135. Geological Society Special Publication, pp. 327–340.

Díaz de Neira, J.A., Solé Pont, F.J., 2002. Precisiones estratigráficas sobre el Neógeno de la Cuenca de Azua (República Dominicana). Acta Geológica Hispánica 37, 163–181.

Dickinson, W.R., Seely, D.R., 1979. Structure and Stratigraphy of Forearc Regions. American Association of Petroleum Geologists Bulletin 63, 2–31.

Dolan, J.F., Mann, P., De Zoeten, R., Heubeck, C., Shiroma, J., Monechi, S., 1991. Sedimentologic, stratigraphic and tectonic synthesis of Eocene-Miocene sedimentary basins. In: Mann, P., Draper, G., Lewis, J. (Eds.), Geologic and Tectonic Development of the North America-Caribbean Plate Boundary Zone in Hispaniola, 262. Geological Society American Special Paper, Hispaniola and Puerto Rico, pp. 217–263.

Dolan, J., Mullins, H., Wald, D., 1998. Active tectonics of the north-central Caribbean region: oblique collision, strain partitioning and opposing slabs. In: Dolan, J., Mann, P. (Eds.), Active Strike-Slip and Collisional Tectonics of the Northern Caribbean Plate Boundary Zone in Hispaniola, 326. Geological Society American Special Paper, pp. 1–61.

Donnelly, T.W., 1994. The Caribbean sea floor. In: Donovan, S.K., Jackson, T.A. (Eds.), Caribbean Geology: An Introduction. U.W.I. Publ Assoc, , Kingston, pp. 41–64.

Donnelly, T.W., Beets, D., Carr, M.J., Jackson, T., Klaver, G., Lewis, J., Maury, R., Schellenkens, H., Smith, A.L., Wadge, G., Westercamp, D., 1990. History and tectonic setting of Caribbean magmatism. Geological Society of America. In: Dengo, G., Case, J. (Eds.), The Caribbean Region, Vol. H. The Geology of North America, pp. 339–374.

Draper, G., Mann, P., Lewis, J.F., 1994. Hispaniola. In: Donovan, S.K., Jackson, T.A. (Eds.), Caribbean Geology: An Introduction. University of the West Indies Publishers Association, Kingston, Jamaica, pp. 129–150.

Escuder Viruete, J., 2004. Petrología y Geoquímica de Rocas Ígneas y Metamórficas del Proyecto K (Sysmin): Hojas de Dajabón, Martín García, Loma de Cabrera, Santiago Rodríguez, Monción, Restauración, Jicomé, Bánica, Arroyo Limón y Lamedero. Informe Complementario al Mapa Geológico de la República Dominicana a E. 1:50.000. IGME-BRGM-INYPSA, Santo Domingo, 130 pp.

Escuder Viruete, J., Contreras, F., Stein, G., Urien, P., Joubert, M., Bernardez, E., Hernáiz Huerta, P.P., Lewis, J., Lopera, E., Pérez-Estaún, A., 2004. La secuencia magmática Jurásico Superior-Cretácico Superior en la Cordillera Central, República Dominicana: sección cortical de un arco-isla intraoceánico. Geo-Temas 6 (1), 41–44.

Feigenson, M., 1978. Petrology and strontium isotope geochemistry of the loma Cabrera batholith, Dominican Republic. MSc thesis. George Washington University, 99 pp.

Fitch, J.T., 1972. Plate convergence, transcurrent faults, and internal deformation adjacent to Southeast Asia and the Western Pacific. Journal of Geophysical Research 77, 4432–4460.

Fossen, H., Tikoff, B., 1998. Extended models of transpression and transtension, and application to tectonic setting. In: Holdsworth, R.E., Strachan, R.A.,

Dewey, J.F. (Eds.), Continental Transpressional and Transtensional Tectonics, 135. Geological Society Special Publication, pp. 15–33.

Gradstein, F.M., Ogg, J.G., Smith, A.G., 2004. A geologic time scale 2004. Cambridge University Press, 610 pp.

Hernaiz Huerta, P.P., Pérez-Estaún, A., 2002. Estructura del cinturón de pliegues y cabalgamientos de Peralta, República Dominicana. Acta Geologica Hispánica 37, 183–206.

Holland, T., Blundy, J., 1994. Non-ideal interactions in calcic amphiboles and their bearing on amphibole-plagioclase thermometry. Contributions to Mineralogy and Petrology 116, 433–447.

Hutton, D.H.W., 1988. Granite emplacement mechanisms and tectonic controls: inferences from deformation studies. Transactions of the Royal Society of Edinburgh: Earth Sciences 79, 245–255.

Hutton, D.H.W., Reavy, R.J., 1992. Strike-slip tectonics and granite petrogenesis. Tectonics 11, 960–967.

Ingram, G.M., Hutton, D.H.W., 1994. The Great Tonalite Sill; emplacement into a contractional shear zone and implications for Late Cretaceous to early Eocene tectonics in Southeastern Alaska and British Columbia. Geological Society of America Bulletin 106, 715–728.

Jarrard, R.D., 1986. Terrane motion by strike-slip faulting of forearc slivers. Geology 14, 780–783.

Joubert, M., Urien, P., ArdévolLl., Bourdillon, Ch., Bonnemaison, M., Escuder Viruete, J., Le Goff, E., Lerouge, C., Escuer, J., Lopera, E., Antón Pacheco, C., García Lobón, J.L., Mortensen, J.K., Ullrich, T., Friedman, R., 2004. Mapa Geológico de la República Dominicana a E. 1:50.000, Lamedero (5973-I). Dirección General de Minería, Santo Domingo, 192 pp.

Kesler, S.E., Sutter, J.F., Barton, J.M., Speck, R.C., 1991. Age of intrusive rocks in Northern Española. In: Mann, P., Draper, G., Lewis, J.F. (Eds.), Geologic and Tectonic Development of the North America-Caribbean Plate Boundary in Española. Geological Society of America Special Paper 262, pp. 165–172.

Kretz, R., 1983. Symbols for rock-forming minerals. American Mineralogist 68, 277–279.

Lallemand, S., Liu, C.-S., Domínguez, S., Schnle, P., Malavieille, J., the ACT scientific crew, 1999. Trench-parallel stretching and folding of forearc basins and lateral migration of the accretionary wedge in the southern Ryukyus: a case of strain partition caused by oblique convergence. Tectonics 18 (2), 231–247.

Lapierre, H., Dupuis, V., de Lepinay, B.M., Bosch, D., Monie, P., Tardy, M., Maury, R.C., Hernandez, J., Polve, M., Yeghicheyan, D., Cotten, J., 1999. Late Jurassic oceanic crust and upper cretaceous Caribbean plateau picritic basalts exposed in the Duarte igneous complex, Hispaniola. Journal of Geology 107, 193–207.

Lewis, J.F., 1982. Granitoid Rocks in Española. Transactions of the 9th Caribbean Geological Conference. Amigo del Hogar Publishers, Santo Domingo. 403–408.

Lewis, J.F., Draper, G., 1990. Geological and tectonic evolution of the northern Caribbean margin. In: Dengo, G., Case, J.E. (Eds.). Geological Society of America, The Geology of North America, Vol. H, The Caribbean Region, pp. 77–140.

Lewis, J.F., Escuder Viruete, J., Hernaiz Huerta, P.P., Gutiérrez, G., Draper, G., 2002. Subdivisión Geoquímica del Arco Isla Circum-Caribeño, Cordillera Central Dominicana: Implicaciones para la formación, acreción y crecimiento cortical en un ambiente intraoceánico. Acta Geológica Hispánica 37, 81–122.

Ludwig, K.R., 2003. Isoplot 3.00, A Geochronological Toolkit for Microsoft Excel. Berkeley Geochronology Center. Special Publication No. 4.

Mann, P., 1999. Caribbean sedimentary basins: classification and tectonic setting from Jurassic to Present. In: Mann, P. (Ed.), Caribbean Basins, 4. Sedimentary Basins of the Word, pp. 3–31.

Mann, P., Draper, G., Lewis, J.F., 1991. An overview of the geologic and tectonic development of Española. In: Mann, P., Draper, G., Lewis, J.F. (Eds.), Geologic and Tectonic Development of the North America-Caribbean Plate Boundary in Española. Geological Society of America Special Paper 262, pp. 1–28.

Mann, P., Taylor, F., Edward, L., Ku, T., 1995. Actively evolving microplate formation by oblique collision and sideways motion along strike-slip faults: an example from the northern Caribbean plate margin. Tectonophysics 246, 1–69.

McCaffrey, K.J.W., 1992. Igneous emplacement in a transpressive shear zone. In: Ox Mountains igneous complex, 149. Journal of the Geological Society, London. 221–235.

Megard, F., 1987. Structure and evolution of the Peruvian Andes. In: Schaer, J.P., Rodgers, J. (Eds.), The Anatomy of Mountain Ranges. Princeton University Press, pp. 179–210.

Montgomery, H., Pessagno, E.A., 1999. Cretaceous microfaunas of the Blue mountains, Jamaica, and of the Northern and Central Basement Complexes of Hispaniola. Caribbean. In: Mann, P. (Ed.), Caribbean Basins, 4(10). Sedimentary Basins of the Word, pp. 237–246.

Passchier, C.W., Trouw, R.A.J., 1996. Microtectonics. Springer Verlag, 289 pp.

Paterson, S.R., Vernon, H.R., Tobisch, O.T., 1989. A review of criteria for the identification of magmatic and tectonic foliations in granitoids. Journal of Structural Geology 11, 349–363.

Petford, N., Atherton, M.P., 1992. Granitoid emplacement and deformation along a major crustal lineament: the Cordillera Blanca, Peru. Tectonophysics 205, 171–185.

Renne, P.R., Swisher, C.C., Deino, A.L., Karner, D.B., Owens, T., DePaolo, D.J., 1998. Intercalibration of standards, absolute ages and uncertainties in $^{40}Ar/^{39}Ar$ dating. Chemical Geology 145, 117–152.

Stein, G., ArdévolLl., Bourdillon, Ch., Bonnemaison, M., Escuder Viruete, J., Le Goff, E., Escuer, J., Lopera, E., Antón Pacheco, C., García Lobón, J.L., Mortensen, J.K., Ullrich, T., Friedman, R., 2004. Mapa Geológico de la República Dominicana a E. 1:50.000, Restauración (5873-I). Dirección General de Minería, Santo Domingo, 168 pp.

Teyssier, C., Tikoff, B., Markley, M., 1995. Oblique plate motion and continental tectonics. Geology 23, 447–450.

Tikoff, B., Greene, D., 1997. Stretching lineations in transpressional shear zones. Journal of Structural Geology 19, 29–39.

Tikoff, B., De Saint Blanquat, M., 1997. Transpressional shearing and strike-slip partitioning in the Late Cretaceous Sierra Nevada magmatic arc, California. Tectonics 16, 442–459.

Tikoff, B., Matthew, T., Davisb, R., Teyssier, C., De Saint Blanquat, M., Habertc, G., Morgand, S., 2005. Fabric studies within the Cascade Lake shear zone, Sierra Nevada, California. Tectonophysics 400, 209–226.

Urien, P., Joubert, M., Ardévol, Ll, Bourdillon, Ch., Bonnemaison, M., Escuder Viruete, J., Lerouge, C., Escuer, J., Lopera, E., Antón Pacheco, C., García Lobón, J.L., Mortensen, J.K., Ullrich, T., Friedman, R., 2004. Mapa Geológico de la República Dominicana a E. 1:50.000, Dajabón (5874-I). Dirección General de Minería, Santo Domingo, 231 pp.